A subaquatic moraine complex in overdeepened Lake Thun (Switzerland) unravelling the deglaciation history of the Aare Glacier

S.C. Fabbri[1*], M.W. Buechi[2], H. Horstmeyer[3], M. Hilbe[2], C. Hübscher[4], C. Schmelzbach[3], B. Weiss[4], F.S. Anselmetti[2]

[1] Institute of Geological Sciences, Baltzerstrasse 1+3, 3012 Bern, Switzerland

[2] Institute of Geological Sciences, Oeschger Centre of Climate Change Research, University of Bern, Baltzerstrasse 1+3, 3012 Bern, Switzerland

[3] Institute of Geophysics, Dept. of Earth Sciences, Sonneggstr. 5, ETH Zürich, CH-8092, Zürich, Switzerland

[4] Institute of Geophysics, Center for Earth System Research and Sustainability, University of Hamburg, Bundesstr. 55, D-20146 Hamburg, Germany

*Corresponding author

Abstract

To investigate the history of the Aare Glacier and its overdeepened valley, a high-resolution multibeam bathymetric dataset and a 2D multi-channel reflection seismic dataset were acquired on perialpine Lake Thun (Switzerland). The overdeepened basin was formed by a combination of tectonically predefined weak zones and glacial erosion during several glacial cycles. In the deepest region of the basin, top of bedrock lies at ~200 m below sea level, implying more than 750 m of overdeepening with respect to the current fluvial base level (i.e. lake level). Seismic stratigraphic analysis reveals the evolution of the basin and indicates a subaquatic moraine complex marked by high-amplitude reflections below the outermost edge of a morphologically distinct platform in the southeastern part of the lake. This stack of seven subaquatic terminal moraine crests was created by a fluctuating, "quasi-stagnant" grounded Aare Glacier during its overall recessional phase. Single packages of overridden moraine crests are seismically distuinguishable, which show a transition downstream into prograding clinoforms with foresets at the ice-distal slope. The succession of subaquatic glacial sequences (foresets and adjacent bottomsets) represent one fifth of the entire sedimentary thickness.

Exact time constraints concerning the deglacial history of the Aare Glacier are very sparse. However, existing [10]Be exposure ages from the accumulation area of the Aare Glacier and radiocarbon ages from a Late-Glacial lake close to the outlet of Lake Thun indicate that the formation of the subaquatic moraine complex and the associated sedimentary infill must have occurred in less than 1,000 years, implying high sedimentation rates and rapid disintegration of the glacier.

These new data improve our comprehension of the landforms associated with the ice-contact zone in water, the facies architecture of the sub- to proglacial units, the related depositional processes, and thus the retreat mechanisms of the Aare Glacier.

1. Introduction

The evolution of the Quaternary landscape and the formation of Alpine valleys has been of scientific interest for generations of geologists over the last 200 years (e.g. Escher, 1820; Penck, 1905), seeking for explanations that elucidate the creation of perialpine lakes and overdeepened troughs (Bini et al., 1978; Finckh, 1978). In recent years, glacial overdeepenings attracted economic interest, since a majority of these troughs host aquifers with drinking water, and major engineering and tunneling projects across the Alps encountered unexpected challenges with the sedimentary infill and morphology of them (e.g. Lötschberg railway tunnel, Schlüchter, 1979). Furthermore, the Swiss nuclear waste disposal program aims at finding a safe repository for high-level nuclear waste that endures future glacial cycles, which requires an improved understanding of factors controlling glacio-fluvial erosion, overdeepening processes and glacial advances and retreat phases of the local Aare, Rhine and Rhone Glacier system (Preusser et al., 2010).

The important role of perialpine lakes for the unravelling of the (de-) glaciation history of the Alps was already recognized by Heim (1894) in Lake Lucerne (Switzerland). The detailed sedimentary archives of lakes serve as excellent trackers of glacial evolution. Moreover, morphological features, which are sometimes hard to identify on land, are perfectly preserved in lacustrine and marine environments, where erosional processes are strongly hampered. Examples of subaquatic glacial morphologies have been shown for example in the fjord basin of Lake Melville, southeast Labrador, Canada (Lønne and Syvitski, 1997), in Lago Fagnano, southern Patagonia (Waldmann et al., 2010), or in central Sweden, where a series of subaquatic end moraines is reported (Johnson et al., 2013).

The global Last Glacial Maximum (LGM, Mix et al., 2001; Clark et al., 2009; Hughes et al., 2013) does temporally fairly well coincide with the maximum reach out of Alpine piedmont glaciers into the northern foreland and the creation of the Italian amphitheatres in the south between 26 ka and 19 ka (Ivy-Ochs, 2015; Monegato et al., 2017, Fig. 1A). The maximum ice extent of the Rhone Glacier, was reached at or slightly before 24.0 ± 1.1 ka, as reported by Reber et al. (2014). They dated the abandonment of the Rhone Glacier's maximum position to 19.1 $\pm$ 1.5 ka, in response to an initial pre-Bølling deglacial phase, which is in good agreement with the onset of deglaciation of the Aare Glacier (Akcar et al., 2011). It seems that Alpine glaciers act very sensitively to slight snowline changes and therefore respond rapidly to temperature changes, collapsing faster during warming pulses (Ivy-Ochs et al., 2004).

The Quaternary landscape created by the Aare Glacier between Bern and the accumulation area at Grimselpass was first described by Penck and Brückner (1909). Beck (1920-1922) noticed that the complete excavation of sedimentary infill in an overdeepened valley during the Würmian glaciation is rather unlikely. The records from drilling sites at Meikirch NW of Bern (Welten, 1988) and at Thalgut (Schlüchter, 1989b, Fig. 1B) north of Thun serve as ideal Quaternary archives to support his claim. The latter reveals top of Molasse bedrock at 147 m depth below surface with at least three glacial

85   cycles covering it (Schlüchter and Kelly, 2000). A basal glacial unit is followed by the lowermost

86   lacustrine clays being indicative for the Holstein Interglacial associated with MIS 9 (Schlüchter,

87   1989b, 1989a). This implies that bedrock erosion to the current level occurred during the glaciation in

88   MIS 10 or even earlier at Thalgut. The sequence is topped with a basal lodgment till deposited during

89   LGM (Preusser and Schlüchter, 2004). At Meikirch, deposits of previous glacial cycles are preserved

90   as well, and the last time bedrock experienced ice contact was during MIS 8 or earlier based on the re-

91   interpretation of sediment logs, palynological correlation and luminescence dating (Preusser et al.,

92   2005). Other drill holes within overdeepened basins revealed similar deposits of previous glacial

93   cycles and showed their preservation potential over several glaciations (e.g. Salzach, Germany: (e.g

94   Niederweningen, Switzerland: Anselmetti et al., 2010; Dehnert et al., 2012; Salzach,

95   Austria/Germany: Fiebig et al., 2014; Lower Glatt Valley, Switzerland: Buechi et al., 2017).

96   In contrast to our fairly good understanding of the ice extent during LGM along the Alps (Fig. 1A), the

97   deglaciation history of the LGM is still poorly constrained and mostly based on ice-marginal

98   landforms, trimlines, striae, roches moutonnées, polished bedrock and erratic boulders (e.g. Jäckli,

99   1962; Schlüchter, 1988). More recent studies in the Upper Aare Valley incorporate surface exposure

100 ages derived from in-situ produced cosmogenic nuclides such as ^{10}Be in boulders and bedrock (e.g.

101 Ivy-Ochs and Kober, 2008; Akcar et al., 2011). Kelly et al. (2006) and Wirsig et al. (2016)

102 reconstructed the retreat and stagnant episodes of the Aare Glacier during its recessional phase from

103 the abandonment of its LGM position northeast of Bern to its accumulation area at Grimselpass using

104 ^{10}Be. The rapid ice decay in the northern foreland (Schlüchter, 1988) hardly left any obvious moraines

105 hinting at a stabilization of the ice front or a Late-Glacial readvance beyond the inner-Alpine regions

106 (Kelly et al., 2006; Reitner et al., 2016). Ivy-Ochs et al. (2006) also notes that, despite detailed

107 geologic mapping for more than 100 years, Gschnitz moraines (Kerschner et al., 1999) have not been

108 found yet in major longitudinal valleys within the Alps.

109 Our extensive multi-channel reflection seismic survey combined with multibeam swath bathymetry on

110 Lake Thun enable us to perform a detailed study of the bedrock topography and the sedimentary infill

111 of its overdeepened basin, both containing several glacial features. We present the seismic stratigraphy

112 displaying the detailed internal structure of a previously unknown large subaquatic moraine complex,

113 including a model that gives a relative chronology of its build-up. Our findings shed new light on the

114 understanding of the deglaciation history of the Aare valley, and will address some challenges

115 associated with the often poorly constrained estimation of overdeepening in perialpine lakes.

116 **1.1. Geological setting**

117 Perialpine Lake Thun lies at the northern front of the Alpine nappes and is situated in the upper Aare

118 valley between Interlaken and Bern (Fig. 1A). Its overdeepened basin is located within sedimentary

119 Penninic and Helvetic thrust nappes and the Subalpine Molasse outcropping on the southwest,

4

120   northeast and northern shores, respectively. The main part of the Lake Thun basin is elongated

121   orthogonal to the general strike direction of the Alpine front (WSW-ENE).

122   During the Pleistocene glaciations, subglacial erosion formed overdeepenings and shaped the study

123   area (Haeuselmann et al., 2007; Reber and Schlunegger, 2016). Ice thickness of the valley glacier may

124   have varied between these different glaciations, but must have reached several hundred meters of ice

125   (ice elevation at ~1200 m a.s.l at Thun and 3000 m a.s.l. at the accumulation area of the Aare Glacier)

126   during the LGM (Bini et al., 2009). Prominent glacial landforms attributed to the last glacial period are

127   limited to the southern shoreline of the lake (Fig. 1C), where a number of relatively continuous lateral

128   moraine ridges run parallel to the lake axis. Furthermore, a drumlin field and ribbed moraines have

129   been described in the area W of Thun (Beck, 1933; Fiore, 2007).

130

6
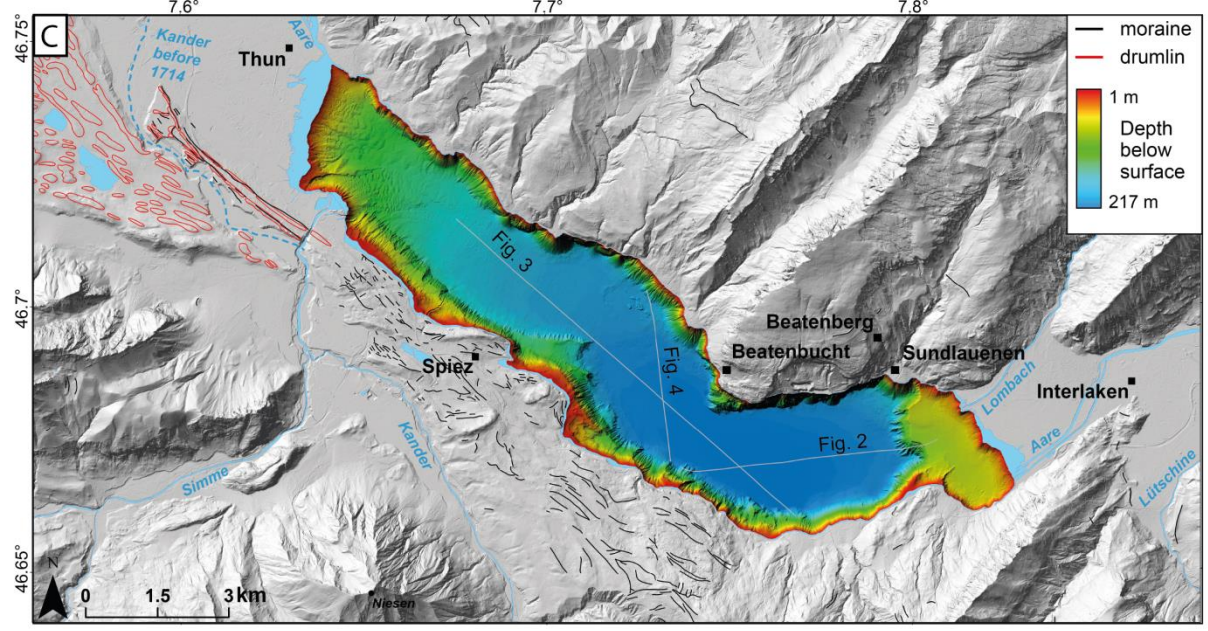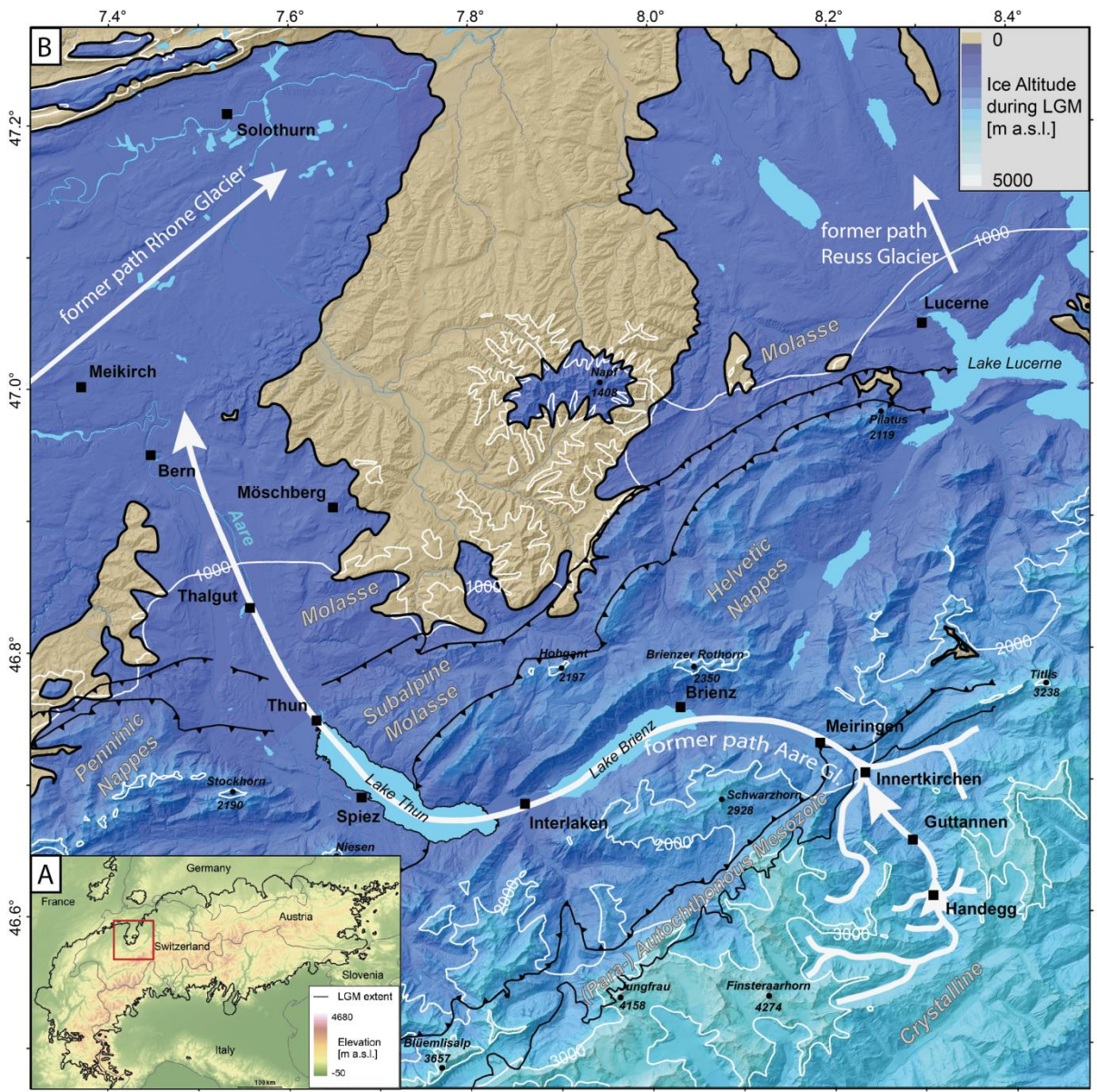
131 *Fig. 1A) Ice extent covering the Alps during the Last Glacial Maximum (LGM). Extent of the ice sheet*

132 *is taken from Ehlers and Gibbard (2004). Elevation data created from SRTM 1 Arc-Second (courtesy*

133 *of the U.S. Geological Survey). B) Hill-shade of digital elevation model (swissALTI3D from swisstopo)*

134 *with ice altitude during LGM superimposed (Bini et al., 2009). White contour lines mark relief*

135 *elevation. Lake Thun was covered by 650 m (Thun) to 850 m (Interlaken) of ice with respect to current*

136 *lake level. Former glacial path is indicated (white line), arrowheads show Gschnitz and Egesen*

137 *stadial positions during deglaciation (Wirsig et al., 2016). The main tectonic units are labelled. Red*

138 *rectangle in A) shows extent of map. C) Hill-shade of digital elevation model with swath bathymetry of*

139 *Lake Thun and some of the most prominent glacial landforms (GeoCover dataset, swisstopo).*

1.2. Previous seismic surveys

141 A first seismic study on Lake Thun was performed by Matter et al. (1971), following the technical

142 recommendations of Hinz et al. (1970) who had previously used the same equipment to investigate

143 Lake Zurich in 1968. The successful imaging and interpretation of the bedrock surface in Lake Thun

144 resulted in a structural map of the basin. They noticed that the deepest part of the lake coincides with a

145 local, spatially well confined depression in bedrock topography to more than 500 m below lake level,

146 adjacent to a shallow-water platform towards Interlaken, where bedrock was interpreted at ~100 m

147 depth below water surface. Drill hole lithology at Interlaken Hospital, however, revealed at that depth

148 the transition between lake sediments and older gravels and sands (Bodmer et al., 1973). In contrast,

149 Bodmer et al. (1973) interpreted bedrock at 300 m below surface in their onshore seismic refraction

150 campaign on the western edge of the Interlaken plateau. Independent of the bedrock depth

151 underestimation, Matter et al. (1971) recognized in their seismic data a few distinct seismic

152 stratigraphic horizons: a shallow one between 7–10 m below the lake bottom, which was attributed to

153 the impact of the Kander deviation from 1714 CE, and two additional ones at 90 and 130 m in the

154 northwestern part of the lake and 100 and 190 m in the deep lake basin. They suggest that the oldest

155 deposits in the Lake basin have pre-LGM ages, as it was subsequently shown for the deposits at

156 Thalgut between Thun and Bern (Schlüchter, 1989b).

157 Finckh et al. (1984) surveyed 17 perialpine lakes using air-gun seismic reflection profiles in

158 combination with sonobuoy refraction measurements in order to evaluate the importance of glacial

159 erosion for perialpine lake formation and the preservation potential of pre-LGM deposits. They single

160 out a few distinctive horizons and assign an overall stratigraphic pattern across all perialpine lakes,

161 which consists of an upper and lower glacio-lacustrine infill and bedrock. In some cases, as for Lake

162 Thun, they split the lower glacio-lacustrine infill into three subunits. The thickness and seismic

163 velocities ranging from 1450 m/s (water column) to 2330 m/s (lowermost sedimentary infill) are in

164 good agreement with this study (see Table 1). They conclude that the erosion of bedrock can be

165 assigned to older glacial periods, since the glacial advance during LGM overrode older glacio-

166 lacustrine deposits revealing only slight loading and erosion, so that deposits of previous glacial cycles

167 are preserved.

168 The upper 60 m of the sedimentary infill of Lake Thun have been described in detail by Wirth et al.

169 (2011) using high-resolution single-channel pinger data. The artificial deviation of the Kander River in

170 1714 CE created a sudden increase in sediment supply to Lake Thun, the formation of a new delta, the

171 accumulation of sediment on existing delta slopes and hence a frequency increase in mass-movement-

172 related turbidites which are represented by large units of a chaotic/transparent seismic facies.

173 *Table 1: Overview of seismic campaigns on Lake Thun. * Assuming sufficient signal power in the*

174 *filtered frequency range and a velocity of 1500 m/s (Rayleigh's criterion of λ/4; e.g. Widess, 1973).*

Acquisition year	1969	1984?	2007	2015
Source type & vol. [cm^3] *refraction*	Air gun 100–200	Air gun 83 *83–655*	3.5 kHz pinger	2-chamber air gun 2 x 245.8
Shot interval [s]	1	5–7	0.5	10
Survey type	Reflection	Reflection & *Refraction*	Reflection	Reflection
# of channels, streamer length (spacing)	1, -	?, 15	1, -	24, 92 (4 m)
BP freq. filtering [Hz]	-	50–600 *20–50*	2200–6300	52-80-1500-2200
Vel. analysis, interval Vel. for infill [m/s]	None, 1500	*Refraction, 1450–2330*	None, 1450	NMO-analysis, 1430–2100
Vert. resolution [m]	?	0.6–7.5*	0.1–0.2	0.7–2.5
Shot spacing [m] at speed [m/s]	1.4–2.5 at 1.4–2.5	?	0.55 at 1.1	(2m CMP distance)
Total profile length	102 km	?	70 km	183.5 km
Publication	Matter et al. (1971)	Finckh et al. (1984)	Wirth et al. (2011)	this publication

2. Methods

2.1. Reflection seismic survey

Acquisition

178 We conducted a multi-channel reflection seismic survey on Lake Thun and used a Sercel two-chamber

179 Mini GI airgun (15/15 in^3) in combination with a Geometrics MicroEel streamer of 97 m length and 24

180 channels (4 m channel distance with 3 hydrophones per channel) as acquisition tools and recorded 42

181 lines with over 180 km total length. Recording of seismic data was nonstop and turns were included

182 into the interpretation software up to 90° deviation from the main course of each line. In order to

183 supplement quality control and data interpretation, brute-stacks were analyzed with a bin width of 12
184 m, bin distance of 4 m, low and high cut-off frequencies of 20–30 Hz and 1000–1500 Hz respectively,
185 NMO of 1500 m/s and time migration.

186 Table 1 gives an overview of all seismic campaigns carried out on Lake Thun. The setup used in this
187 survey overcomes the drawbacks of limited resolution and penetration depth, using state-of-the-art
188 equipment and processing work flow. Shot time interval was 10 seconds at 6.6 km/h survey speed,
189 resulting in an average shot spacing of 18 m and an assigned common-mid point (CMP) interval of 2
190 m, corresponding to half the receiver spacing. The frequency spectra show reasonable signal power up
191 to 500 Hz, resulting in a vertical resolution of the topmost stratigraphic sequences of $\lambda/4 = 0.7$ m. An
192 average theoretical vertical resolution of $\lambda/4 = 2.5$ m is obtained, when using a velocity of 1500 m/s
193 and a main frequency of 150 Hz (Widess, 1973; Chopra et al., 2006) . The GI gun yielded significanty
194 higher resolution when compared to previous airgun surveys (e.g. Finckh et al., 1984). The position of
195 the survey vessel was tracked with a Garmin GPSmap76Cx GPS receiver recording one point every 2
196 s with 2–5 m accuracy. Since the survey velocity was kept constant during acquisition, the easting and
197 northing positions were individually smoothed and interpolated to 1 s. The smoothing was done with a
198 local regression using weighted linear least square and a first degree polynomial model. Shot timing
199 was recorded with an onboard GPS clock. After CMP assignment, the tracks were Kalman-filtered
200 before integration into the interpretation software *SMT Kingdom Suite 2015*.

201 *Processing*

202 The following processing steps were applied to the seismic data with the processing software
203 *SeisSpace/ProMAX (Halliburton/Landmark)*: frequency bandpass filtering, muting, velocity-model
204 creation based on normal-move-out (NMO) analysis and recorded sound-velocity profiles from
205 bathymetric survey, multiple suppression using surface-related multiple elimination (SRME;
206 Verschuur et al., 1992), NMO corrections and CMP stacking, post-stack FX-deconvolution, and post-
207 stack Kirchhoff depth migration.

208 The velocity estimate for the water column was based on the average of 39 P-wave profiles recorded
209 during the bathymetric campaign in September 2014, the direct wave from seismic data and
210 information from a water station at Thun. Only the topmost 40 m of the water column change
211 significantly throughout the year. The velocity in 1 m water depth was calculated from the direct wave
212 travelling along the floating streamer. The estimated velocity is about 1435 m/s based on 5 shots of
213 each survey line. In 5 m water depth, the formula of Wong and Zhu (1995) was applied, which uses
214 temperature [°C], salinity [ppt] and pressure [kPa] as input to calculate sound speed. Salinity was
215 assumed to be zero. Additionally, we consulted the water temperature recordings of the Aare discharge
216 station located close to Lake Thun (3 km downstream from the outlet), which are continuously
217 provided by the Federal Office for the Environment (FOEN). The calculated velocity in 5 m water
218 depth is 1434.2 m/s. The profile between 0 and 70 m was then interpolated in a cubic manner.

219 NMO velocity analysis ideally requires strong continuous horizontal reflections, which is not always

220 given. Velocities for up to 7 reflections (lake bottom to top bedrock) at every 100th to 200th CMP were

221 picked, depending on the length of the profiles and the morphology of the bedrock. Bedrock velocity

222 was kept below 2500 m/s, since the migration algorithm can handle only moderate lateral velocity

223 changes. In overdeepened lake basins where water-saturated low-velocity sediments are in direct

224 contact to bedrock, downward and lateral velocity increases from 1500 m/s to 4000 m/s and higher are

225 common and beyond the capabilities of the migration algorithm. However, our underestimated

226 bedrock velocities affect primarily bedrock-internal structures which are mostly beyond the resolution

227 and focus of our study.

228 Major challenges were encountered close to the shoreline, where water depth is only a few tens of

229 meters and surface-related multiples were difficult to remove, as the SRME algorithm revealed its

230 limitations. Due to the rather short streamer length, the CMP-fold was often as low as 2 or 3, but the

231 low fold had a negligible impact on the image quality due to the high quality of the data.

2.2. Multibeam bathymetry

233 High-resolution bathymetry data of Lake Thun were acquired during 14 days in September and

234 October 2014 (Fig. 1C) using a Kongsberg EM2040 multibeam echo sounder. The positioning system

235 used for the bathymetric campaign was a Leica GX1230 GNSS receiver in combination with the

236 swipos GIS/ GEO real-time kinematic positioning service provided by swisstopo. Survey lines were

237 oriented mostly parallel to the lake's long axis, while areas of shallow water depth (< 15 m) were

238 surveyed in a shore-parallel pattern. Bathymetric data cover most of the lake basin from the deepest

239 areas up to 5 m water depth. The processed point cloud has been rasterized for geomorphologic

240 analysis of the lake floor. The resulting digital bathymetric map has a cell size of 1 m with a vertical

241 accuracy in the order of a few decimeters. Hilbe et al. (2011) and Hilbe and Anselmetti (2014) provide

242 a more detailed review on the acquisition procedure, equipment setup and the use of swath bathymetry

243 tools in lake research.

3. Seismic stratigraphy

3.1. Introduction

246 The overall seismic stratigraphy of Lake Thun shows, from bottom to top, a succession of bedrock,

247 glacial tills, glacio-lacustrine and lacustrine deposits. This general stratigraphy can be further

248 subdivided into ten seismic units (U0–U9), based on characteristic seismic facies, unconformities and

249 predominantly prominent strong reflections (Figs. 2, 3 and 4). However, seismic facies may change

250 within one single unit, but units are not subdivided further for simplicity reasons. All stratigraphic

251 sequences are clearly discernable in the deep basin (Fig. 2), where reflections are laterally continuous

252 and bedrock morphology reveals major overdeepening with steep flanks. Recognition of single

10

253   sequences is impeded when approaching the gas-rich delta deposits of the river Kander and its signal

254   blanking characteristics (Fig. 3). About 400 m beyond the rim of the eastern platform towards

255   Interlaken, signal penetration fades out and the shallow water depth causes strong multiples making it

256   impossible to trace units into the center of the platform. Close to river inlets, gas-rich sediments

257   prohibit good signal penetration as well.

258   Table 2 provides an overview of the seismic stratigraphic interpretation. Since lithological and

259   sedimentological information is lacking, the stratigraphic interpretation is mainly based on

260   hydroacoustic data and derived from morphological, geometric properties of the facies.

261   *Table 2: Seismic stratigraphy in Lake Thun with facies, max. unit thicknesses, geometry description, expected lithology and interpretation.*

Unit	Seismic facies (max. thickness in shallow basin NE/deepest basin SW)	Expected lithology	Interpretation
U9	Similar as U8 (> 100 m on subaquatic platform in the E)	Lacustrine deposits with few turbidites and coarse gravely base with clays intercalated	Similar as U8 with increased fluviatile influence
U8	Parallel, strong continuous horizontal reflections, with semi-transparent intercalated sections (40 m/60 m)	Lacustrine sedimentation (sand to clay) with intercalated turbidites	Increasing *in-situ* sediment production, Holocene
U7	Transparent facies with only gentle horizontal reflections, onlapping (20 m/20 m)	Normally graded layer, possibly pebbles at base	Mass-movement-induced megaturbidite
U6	Parallel, strong continuous reflections with onlap onto U5 or deeper units, amplitudes laterally varying towards NW, faults (~50 m/~50 m)	Mostly sandy silt and mud, strong layering, turbidites	Lacustrine deposits, high sedimentation rate due to proximity of melting glacier
U5 (1A-8A)	High-amplitude reflections with faint internal stratification, layering slightly inclined outside main basin dipping to E	Diamict, sand, gravel, boulders	Build-up of terminal moraine crest of stagnant, or slightly readvancing glacier
U5 (1B-7B)	High-amplitude, continuous reflections in foresets to bottom sets at top of sequence; base of each subunit with rather chaotic facies, few faults rooting in deeper units (20 m/100m)	Mostly sand and glacial mud, with coarse material at the base	Transition from proximal (till) to more distal fine-grained glacio-lacustrine deposition, overall coarsening towards proximal positions
U4	Horizontal reflections with generally low amplitudes, laterally varying, onlapping onto U3, few faults (-/80 m)	Fine laminated muds with dropstones, melt-out from glacier base, deposition from suspensions	Glacio-lacustrine sediments, no ice contact, initiation of deglaciation
U3	Transparent to semi-transparent chaotic facies at the base with faint internal stratification, higher amplitudes towards the top with disturbed layering, many faults, overall similar to U1 (~50 m/~150 m)	Diamict with dropstones at base, fining up with glacial mud towards the top	Waterlain till with shore-parallel eskers on the flanks
U2	Semi-transparent facies at bottom, high-amplitude reflections at the top (especially N of Spiez), strong continuous inclined layering, deformed and eroded by U3, many faults (20 m/50 m)	Bottom: proximal diamict with coarser fraction; Top: fine muds	Partially stratified (deformed) till, eroded by subsequent glacial readvance, ==temporal subglacial lake development==
U1	Transparent to semi-transparent chaotic facies, generally low amplitudes, few faults (-/>160 m)	Diamict, glacial mud with dropstones, coarse gravelly base	Oldest glacial sediments, till, esker-like features on the SW flank of the basin
U0	High-amplitude, laterally continues reflections in NW, low-amplitudes in SE and greater depth, strongly inclined internal reflections	Molasse, limestone, globigerina marls, dolomite, gypsum, clays	Bedrock of subalpine molasses, Penninic and Helvetic nappes

262

3.2. Unit U0 – bedrock

U0 is interpreted to represent the bedrock below the lake. The top of the unit displays numerous morphologic steps and is marked by a series of high-amplitude reflections in the north, fading out towards the south and at greater depth.

The bedrock often comprises inclined reflections typical for Penninic and Helvetic nappes (Wissing and Pfiffner, 2002). Syn- and antiforms occur in the vicinity of the transition from Penninic nappes to Subalpine Molasse in the northwestern part of the basin (Fig. 3). The bedrock surface reveals a complex morphology with the most pronounced incision south of Beatenberg at roughly 750 m below today's lake surface. The incision narrows at Beatenbucht (Fig. 1C), where limestone formations crop out in vertical cliffs, as well as close to the sill at Spiez, where an antiform on land extends into Lake Thun (Fig. 3). Distinct valley troughs, causing a local secondary inset trough within the basin (Fiore et al., 2011), were cut into the bedrock and probably represent erosional imprints of highly erosive subglacial meltwater flows (Menzies and Shilts, 2002; Fig. 4). Fig. 6 shows the surface of the bedrock U0 with depth and morphological information. The deepest point reaches 776 m below lake level (557.48 m a.s.l.) with an elevation of 218 m below sea level. Based on the recorded 42 seismic lines (Fig. 7A), the sedimentary infill was calculated to amount to >560 m in the deepest part of the basin (Fig. 7B).

3.3. Unit U1 – till 1

Unit U1 reveals a broad range of facies and is capped by a rather discontinuous reflection (Fig. 2, etc.). The facies ranges from transparent to semi-transparent with occasional faint internal stratification. U1 overlies bedrock (U0) and is spatially restricted to the deepest part of Lake Thun. It pinches out towards the sill at Spiez (Fig. 7C), filling up a distinct bedrock trough. As in Lake Zurich (Giovanoli et al., 1984), this pattern is interpreted as till lacking coherent reflectors and resulting in a nearly transparent facies.

U1 levels out some of the bedrock channels and shows itself a diverse morphology with local peaks at the flanks. Highly reflective, arc-shaped peaks up to ~15 m in height are stacked on the southeastern flank of line 08 (Fig. 3). These positive subglacial landforms could represent subglacial channel fills, (e.g. eskers), infilled with stratified gravelly deposits (Pugin et al., 1999; Fiore et al., 2011). There are almost no faults recognizable due to limited signal penetration and decreasing resolution with depth.

292
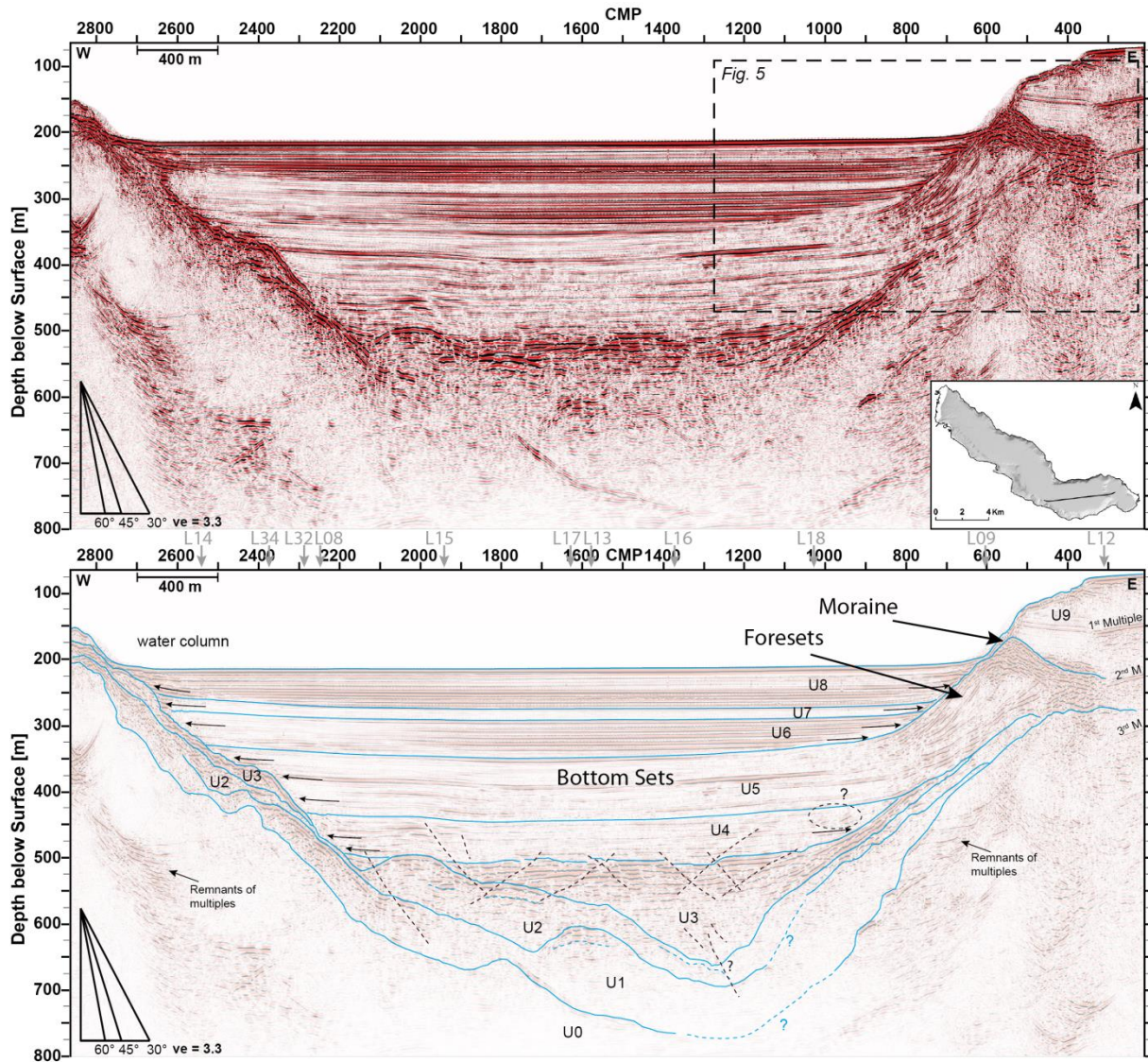
Fig. 2: Seismic inline profile 20 along the deepest section of the basin shows all stratigraphic units interpreted to represent bedrock (U0), sub- to proglacial deposits (U1-U5), and glacio-lacustrine to lacustrine (U6-U9) deposits. The profile track is shown in the inset (top). Beyond the platform in the East, signal loses penetration due to the shallow waters and strong multiples. Remnants of multiples are visible in some other parts of the profile. The moraine and its related foresets and bottom sets in U5 are illustrated in more detail in Fig. 5. Small black arrows mark onlapping. The black question mark highlights inclining layers within horizontal deposits. Many faults populate U2 to U5 (black dotted lines). Grey arrows show intersections with crosslines.

3.4. Unit U2 – (stratified) till 2

Unit U2 is characterized by a general increase of high-amplitude continuous reflections compared to subglacial till unit U1, which is increasingly well-developed towards the top of the unit and in the NW (Fig. 3). While these seismic facies is likely to reflect an internal bedding of unit U2, some similarity with the chaotic facies U1 is apparent.

14

The origin of stratification in tills may be sedimentary or deformational. In overdeepened glacial basins, stratified deposits typically represent either waterlain tills emplaced in a dynamic subglacial to sub-marginal lake setting (see also U3) with temporary loss of glacier ground contact, or alternatively, an incompletely stratified unit U2 due to subglacially deformed and overridden glacio-lacustrine deposits, which preserved some of the initial stratification. 133 individual fault strands penetrate U2 with the majority located in the NW (Fig 3). However, the size of the faults (several tens of meters) is beyond the commonly expected extent for subglacial deformation (range of decimeters, Boulton et al., 2001). The non-uniform thickness of the unit and local troughs suggest that U2 was partially deformed and eroded by a subsequent glaciation (Fig. 2). We suggest both, the combination of a deformational and a sedimentary origin of the stratification, which is indicated by the subhorizontal internal bedding and the infilling character that levels out underlying topographic undulations of U1 and U0. The unit covers the entire basin except the shallow platform close to Interlaken. Since U1 is not present NW of the sill at Spiez, U2 directly overlies the bedrock there. Some patches of U1 occasionally occur SE of the sill at Spiez (Fig. 3). Unit U2 can be therefore interpreted as stratified till in a subglacial environment.

### 3.5. Unit U3 – (waterlain) till 3

Unit U3 shows a transparent to semi-transparent facies at the base with only slight internal stratification. Towards the top of the unit, higher amplitudes start to dominate and the facies change into a similar character as U2. The layering is frequently disturbed by faults. In the deepest part of the basin, the reflections are mostly horizontal, while the deposits on the flanks show a slope-parallel inclination. The base of U3 reaches elevations down to 100 m below sea level in the South. U3 mostly levels out the undulating topography of underlying units. Similar to U1, the highly reflective, arc-shaped peaks occur at the very same flank in profile 08 (Fig. 3) and are up to ~25 m high. They are traceable across several lines with a shore-parallel extension and possibly represent a chain of eskers (Pugin et al., 1999; Fiore et al., 2011).Unit U3 is more extensive than U1 and covers almost the entire basin (Fig. 7D).

The base of U3 is interpreted as the onset of the last glaciation with an erosive base removing partially underlying U2, causing a non-uniform thickness distribution and undulating top of U2, and emplacing a glacial till (Lister et al., 1984). The relatively smooth and continuous top of U3, with a pronounced horizontal character at the deepest section of the basin, therefore indicates terminal deposits that have not been overprinted by a subsequent glacial readvance with deforming ice contact at the base. However, the high amplitudes underlining the horizontal internal layering of U3 in line 20 (Fig. 2) tends to be slightly exaggerated, since some of this horizontality has to be attributed to the partial lack of multiple removal. Nevertheless, the deepest part of the basin is dominated by high-amplitude horizontal reflections, signaling the potential loss of ground contact of the glacier and the onset of the

15

341 development of a subglacial to sub-marginal lake (Fig. 2). Line 08 and 31 in Figs. 3 and 4 illustrate

342 the undulating internal stratification of U3.

343
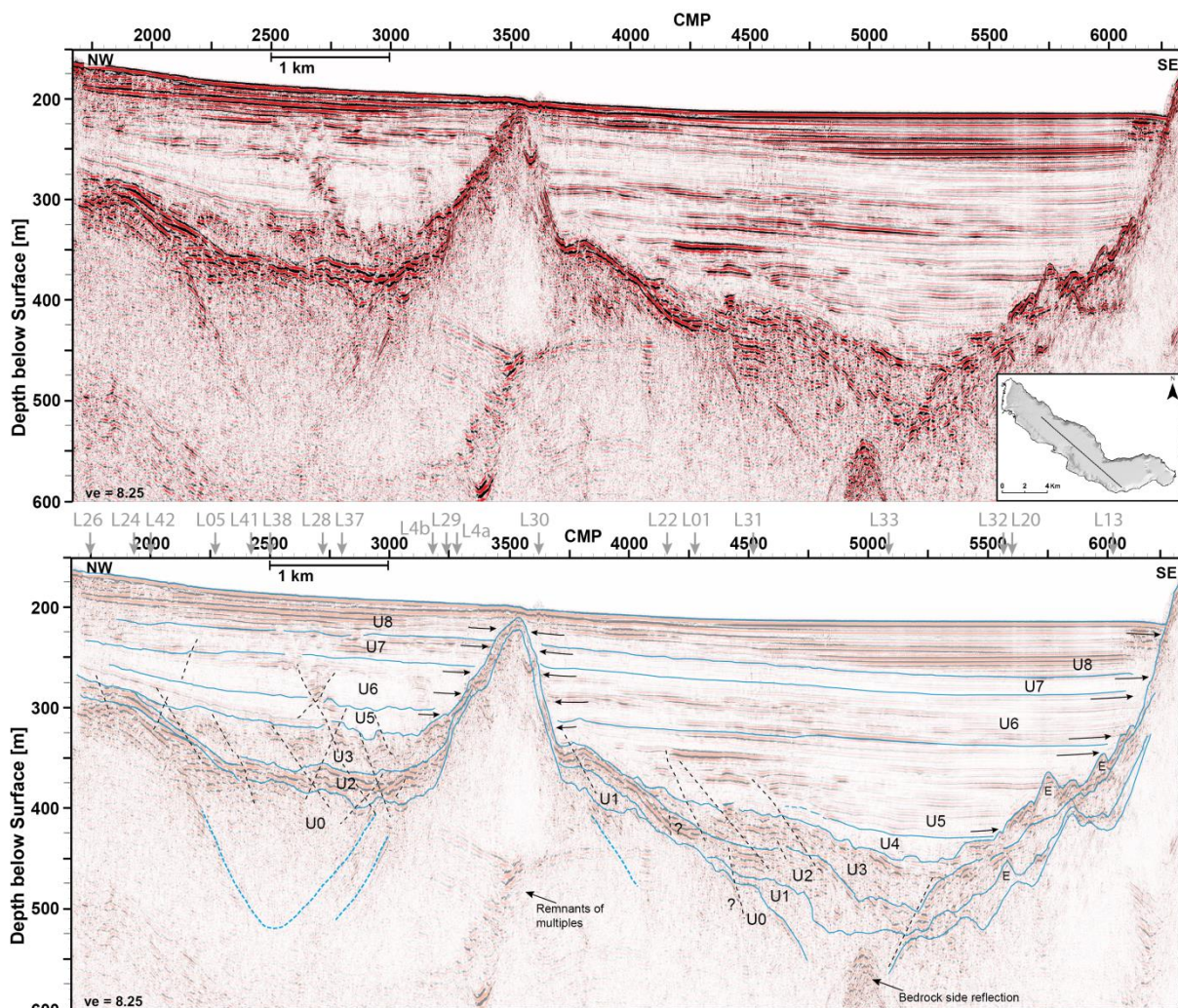
Fig. 3: Seismic inline profile 08 across the sill at Spiez. The profile track is shown in the inset (top).

Towards the NW, signal loses penetration due to gas rich sediments brought by the Kander river. U1

and U4 are missing NW of the sill. Blue dotted lines hint at syn-/antiforms in the bedrock. Black

arrows mark onlapping. "E"s show esker-like structures.

348 Most of the faults observed in our data (167 individual fault strands out of 193 totally identified

349 strands) penetrate U3. About one third of all fault strands are thrust faults with apparent dip angles

350 lower than 35°, and one quarter shows a normal faulting regime. The remaining strands do not allow

351 for a specific faulting regime to be identified or have to be interpreted as strike-slip faults. Brittle

352 faulting is commonly observed in subglacial tills and typically associated with low basal shear

353 stresses and low pore-water pressures. However, the observed faults may be of neotectonic nature

354 rooting in bedrock structures, since the subglacial deformation zone is usually limited to a few

355 decimeters (e.g. Boulton et al., 2001; Piotrowski et al., 2001) and therefore beyond the seismic

356 resolution. Alternatively, the faults may be related to the sediment overload (settlement) induced by

16

the infill or a postglacial rebound as described at a larger scale for the Fennoscandian ice sheet (Muir-Wood, 1989, 2000).

3.6. Unit U4 – post-LGM subglacial lake sedimentation

Unit U4 shows mostly horizontal low-amplitude reflections onlapping onto U3, indicating an abrupt change in the depositional environment. The unit is clearly restricted to the southeastern part of the basin (Figs. 3 and 4) and has a seismic facies comparable to U5.

During deposition of U3, the glacier loses eventually contact with the ground or simply disintegrates and retreats. U4 records the time between a lifted and retreating Aare glacier (U3) and ice-free conditions with the ice front at the subaquatic platform (see U5) or further upstream. Initially, U4 is mostly deposited from rain-out of a melting ice tongue, suspension settling and sediment flows producing finely laminated muds with dropstones (Bennett and Glasser, 2009). In Fig. 2, faint traces of inclined layers are recognizable (marked with a dashed circle), likely related to the onset of clinoform formation (see U5) as it is typical for the sediment dumping in front of a nearby glacial tongue. This depositional regime translates soon thereafter to a glacio-lacustrine to lacustrine environment in a proglacial lake.

3.7. Unit U5 – Sundlauenen subaquatic moraine complex (SMC) and clinoforms

In case of unit U5, the excellent data quality allowed for a further subdivision into subunits 1 to 8, each of them made of a corresponding package characterized by distinct seismic facies, marked with a letter suffix A and B (Fig. 5). The two types of seismic facies and its division into eight subunits are best seen on line 20 (Figs. 2 and 5). Facies A builds arc-shaped crests with high-amplitude reflections with partial internal stratification. It extends from the north to the south shore along the platform edge (inset Fig. 5 bottom). Facies B is characterized by high-amplitude continuous reflections steeply inclined close to the crest and becoming gradually less inclined and eventually horizontally layered in the center of the basin. U5 was deposited over the entire basin (Fig. 7E).

Based on the arc-shaped and dome-like geometry, as well as reflection characteristics, facies A is interpreted as subaquatic moraine complex, hereafter termed Sundlauenen subaquatic moraine complex (SMC), created by a stagnant to periodically readvancing glacier during its overall retreating phase. Its vertical thickness at the peak of the moraine crest amounts to ~130 m. Very similar facies and structures in correspondence with recessional glacial phases are known from lake and fjord settings (e.g. Lønne and Syvitski, 1997; Waldmann et al., 2010; Hilbe et al., 2011).Thrust faults within facies A are likely to form during minor readvances/oscillations when the glacier pushes into the morainal ridges as commonly observed in terminal moraine settings (e.g. Lønne and Syvitski, 1997; Bennett, 2001; Johnson et al., 2013). Similar subaquatic moraine features, documenting
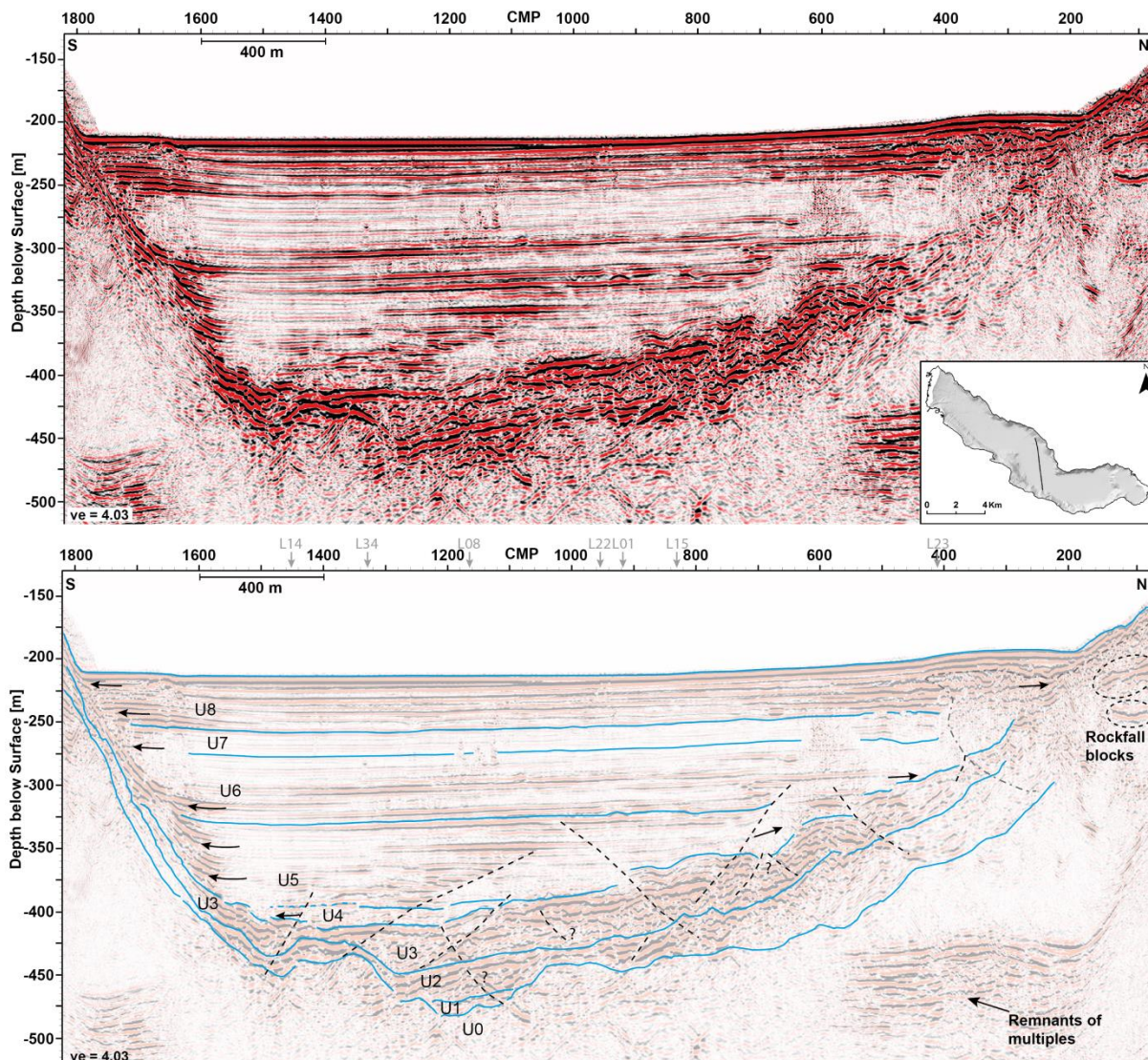
Fig. 4: Seismic crossline profile 31. The profile track is shown in the inset (top). Towards the N, signal loses penetration due to the Ralligen rockfall 588/599 CE (see also Wirth et al., 2011). Blocks of limestone belonging to the rockfall are marked with black dashed circles. The dashed dotted grey line outlines the rockfall affected area. Black arrows mark onlapping and black dashed lines indicate faults.

Facies B is interpreted to be glacio-deltaic clinoforms that originate close to the moraine crest and represent foresets at the ice-distal slope and bottom set beds in the deepest part of the basin.

Subunits A and B are deposited simultaneously (Fig. 5) forming a genetic seismic sequence. Adapting a seismic sequence stratigraphic approach, these subunits can be defined as 'subaquatic glacial seismic sequences', which allow the reconstruction of glacial retreat and advance stages and ice front positions during an ice-grounded moraine formation. Dip angles of the foresets, as well as tratigraphic

18

404 thicknesses increase during the initial phase of the SMC build-up (subunits 1–4) and start to decrease

405 thereafter (subunits 5–7).
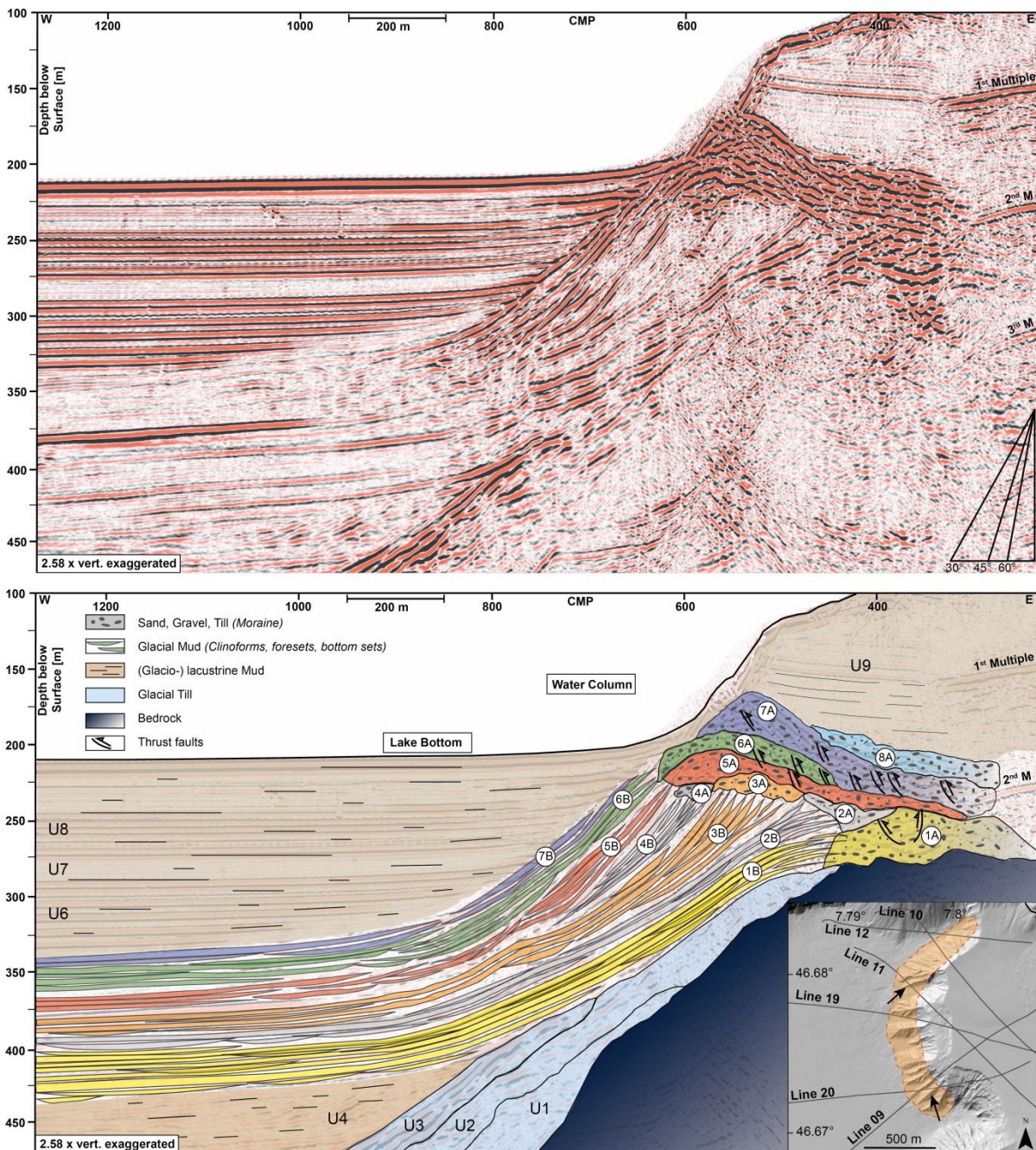
406
407 *Fig. 5: Numerals 1–8 mark individual subdivisions of unit 5 in line 20 (Fig. 2). Corresponding letters*

408 *A,B indicate different facies of subunits. Top: Blue dotted lines mark package boundaries of subunits.*

409 *Inset: Overview of subaquatic moraine extension (orange area) delineated by seismic and swath*

410 *bathymetry data. Upper and lower bounds of orange area are drawn along moraine apexes of 7A*

411 *(seismic) and toe of lake-bottom slope. The orange polygon measures ~200 m across and 1.6 km*

412 *along the arc. Black arrows mark remnants of high-amplitude erosion-resistant moraine crests.*

The combined thickness of U4 and U5 (Fig. 7E) marks the sedimentation during the onset of deglaciation in the deepest part of the basin. It amounts to ~170 m of sediment, which represents a third of the entire sedimentary column.

3.8. Unit U6 – glacio-lacustrine deposits

In the deepest part of the basin, unit U6 is dominated by high-amplitude parallel reflections (Fig. 2), which lose amplitudes towards the flanks. The transparency of the reflections also increases constantly towards the NW (Fig. 3) and the reflections finally fade out entirely when approaching the Kander delta.

The facies of U6 is characteristic for sedimentation in a low-energy, glacio-lacustrine environment. During its formation, the lake is entirely ice-free, and the largest sediment fraction delivered to the lake is provided by glacio-fluvial melt water of the retreating Aare Glacier, and to some minor parts, by smaller tributaries. Initially, the ice front might have been still in contact with the lake water in the form of a floating glacier tongue. However, the basin of Lake Brienz, separated by progradation of a tributary delta (Lombach & Lütschine river) upstream of the subaquatic moraine crest soon becomes an efficient sediment trap and hinders glacio-lacustrine material being transported beyond Interlaken, so that in-situ lacustrine sediment production becomes dominant.

3.9. Unit U7 – megaturbidite

Unit U7 shows a highly transparent seismic facies with only very slight layering. The sharp upper and lower boundaries of the unit (Fig. 2) occur in the deepest part of the basin all the way to the bedrock sill at Spiez. Beyond the sill further northwest, the transparency of the facies is replaced by higher amplitudes (Fig. 3). However, also in the northwestern part, the transparent facies persists, though it is limited to the base of U7. Generally, the unit is deposited across the entire basin apart from the subaquatic platform and the shallow bedrock sill at Spiez (Fig. 7F). The top of U7 reveals a smooth topography.

The highly transparent facies of U7 is typical for turbidites in general, but also for 'megaturbidites' and has been reported in several peralpine lakes such as Lake Como, Italy (Fanetti et al., 2008), Lake Geneva (Kremer et al., 2012) or Lake Lucerne (Schnellmann et al., 2006). The exceptional thickness and large extent clearly classifies it as a 'megaturbidite' (Bouma, 1987). The spatial extent of the 'megaturbidite' with significant thickness change beyond the bedrock sill at Spiez suggests that the sill itself acted as an efficient barrier. The turbidite had to flow around the bedrock barrier significantly slowing it down and leading to the reduced thickness and extent in the northwest (Fig. 3).

The source area of the turbidite is located close to the bedrock escarpment (Fig. 7F, I) where a spatially restricted chaotic facies dominates and penetrates and affects U6 locally. However, the

447   expected massive limestone blocks related to the big escarpment and the ancient rockfall (rockfall at

448   Balmholz, ~0.1 km3, Beck, 1907) are no longer recognizable on seismic data and must have been

449   removed by a former glaciation. Therefore, a subsequent smaller subaerial or subaquatic rockfall most

450   likely caused the 'megaturbidite'. Rockfall-evolved mass-flow deposits and associated

451   'megaturbidites' have been previously reported in other perialpine lakes as in Lake Lucerne

452   (Schnellmann et al., 2006).

453   **3.10. Unit U8 & U9 – lacustrine deposits**

454   Unit U8 is characterized by high-amplitude reflections with small semi-transparent to transparent

455   intercalations. The unit extends over the entire basin and is analyzed and described by Wirth et al.

456   (2011).

457   Unit U9 is limited to the lacustrine deposits on the subaquatic platform close to Interlaken. The

458   seismic facies is comparable with U8 and contains an alternation of high-amplitude reflections and

459   intercalated semi-transparent deposits. Signal penetration in the center of the platform is hampered by

460   the shallow water depth and its associated multiples. This effect is additionally enhanced by gas-rich

461   sediments. Therefore, internal facies and structures of U9 are solely resolved close to the platform

462   edge (Fig. 2).

463   Unit U8 was affected by several mass movements and contains their related turbidites. Mass

464   movements were induced by lake-level fluctuations, floods, nearby earthquakes and delta-slope

465   instabilities (Wirth et al., 2011). Blocks of the Ralligen rockfall in 598/599 CE (Wirth et al., 2011) are

466   visible in the bathymetric data in form of raised limestone blocks surrounded by a semi-circular lobe

467   of squeezed out and deformed lake sediments (Fig. 1C). The blocky and chaotic character of the

468   seismic profiles crossing the mass-movement deposit confirms these observations (Fig. 4). The source

469   area of the associated mass-flow deposit is given in Fig. 7F, II.

470   Similarly, U9 is also influenced by subaquatic mass-movement deposits recognizable in the

471   bathymetric data (Fig. 1C). However, the U8 and U9 stratigraphy are not directly comparable with

472   each other since the moraine complex in U5 acts as a trap and sediment barrier for incoming fluvial

473   material form the east brought by the Aare, Lütschine and Lombach rivers. Especially the latter two

474   delivered a lot of coarse gravely material (Bodmer et al., 1973) and silted up the area at Interlaken,

475   creating a fundament of fluvial deposits in U9 and shifting later towards a lacustrine dominated

476   deposition.

477
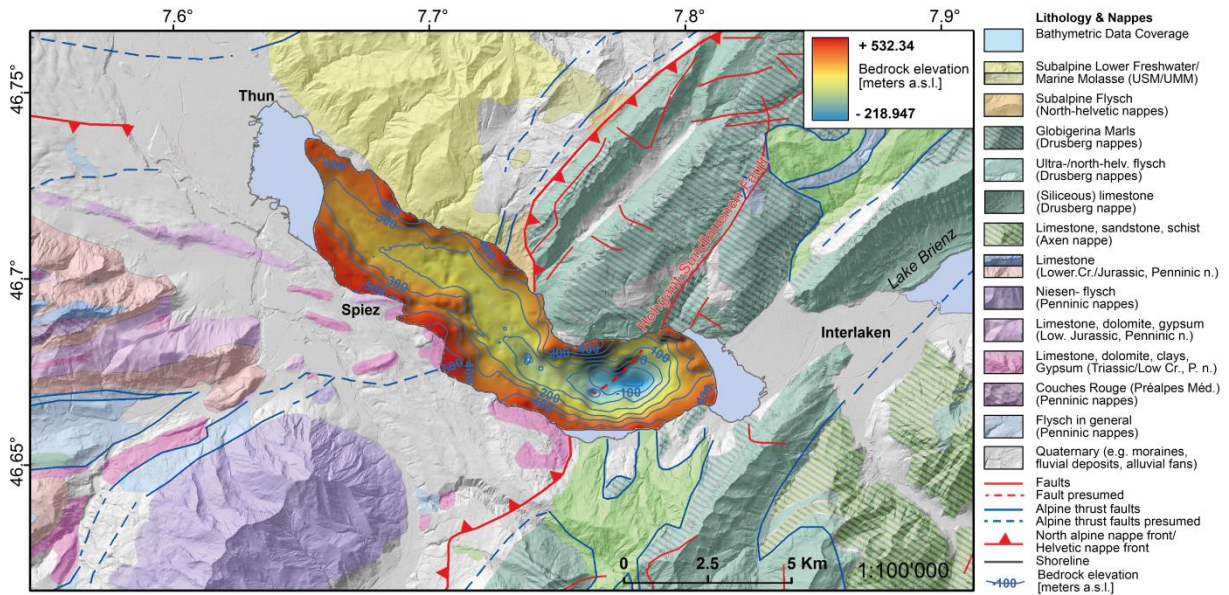
Fig. 6: Hill-shade of digital elevation model (swissALTI3D from swisstopo) with color-coded bedrock map (25 m cell size FlexGridding algorithm, Kingdom Suite 2015) and local geology (simplified Geologie 500 map from swisstopo) superimposed. 100 m contour interval is added for readability. Bright blue zone reflects the data coverage by the bathymetric campaign.
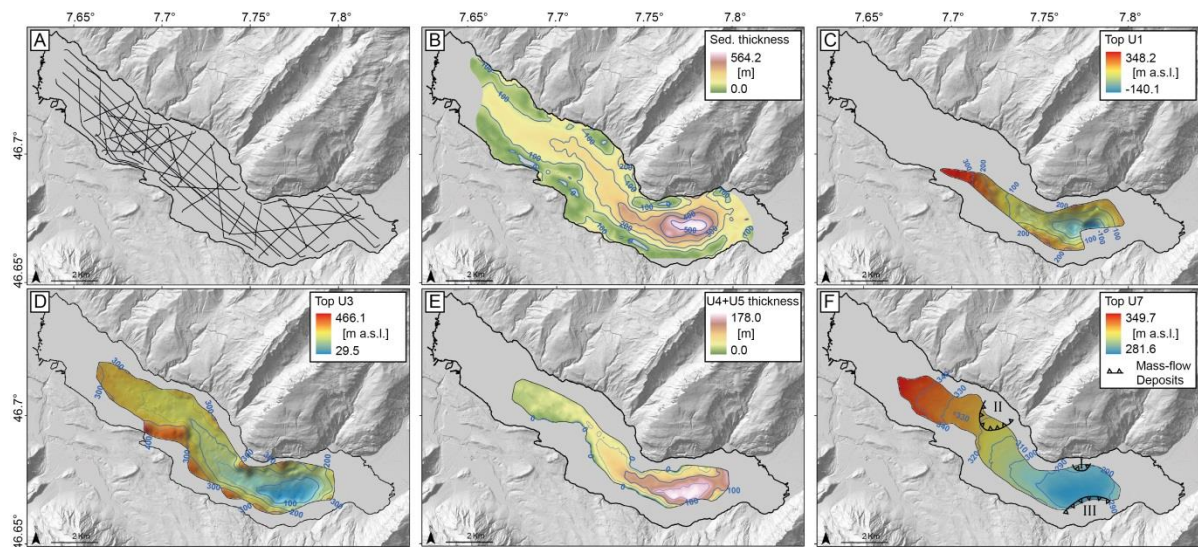
Fig. 7: A) Multi-channel reflection seismic line tracks. B) Calculated sediment thickness based on the difference of swath bathymetry data and the bedrock map; C) Extent and morphology of the top U1, the lowermost till deposits. D) Extent and morphology of the youngest till deposit. E) Thickness of U5, the deltaic clinoforms and its directly underlying sediment U4. U4 is mostly restricted to the deepest basin. F) Extent of top U7. Source area of mass-flow deposit I, II and III are in U7, U8 and U8, respectively. All gridded horizons are limited to the extent of the seismic lines where the corresponding picked horizon was encountered in order to reduce extrapolation of data to a minimum

22

491 *and only interpolate between the lines. We converted all horizons to a 25 m grid (FlexGridding*

492 *algorithm, Kingdom Suite 2015) for the calculations. Thick blue contours show intervals of 100 m,*

493 *except for F) with 10 m intervals.*

4. Discussion

4.1. Bedrock morphology

496 The overall shape of the bedrock surface in the lake basin is in good agreement with the results from

497 (Matter et al., 1971). However, we obtained a significantly larger overdeepening (776 vs. ~550 m) in

498 the deepest section with respect to the current lake/base level at 557.48 m a.s.l. Matter et al. (1971)

499 likely interpreted the strongest reflection as bedrock, which we identified as top of unit U3. The

500 seismic survey of Lake Brienz led to similar values in its deepest section with an overdeepening

501 exceeding 800 m (Matter et al., 1973), even though they used a constant velocity of 1500 m/s, which

502 is assumed to significantly underestimate bedrock depth. Finckh et al. (1984) reported an

503 overdeepening of 605 m for Lake Thun, which is ~150 m less than what we observed for the deepest

504 depression. This deviation is mainly due to the course and orientation of the profile in Finckh et al.

505 (1984), which is slightly offset to the east with respect to the deepest point in bedrock. The massive

506 bedrock depression observed in Lake Thun is in good agreement with many other overdeepened

507 basins in the Alps (e.g. Preusser et al., 2010).

508 The overdeepening of more than 750 m at the deepest point (i.e. −200 m a.s.l, Fig. 6) in the Lake

509 Thun basin (with lake level as reference) can be attributed to multiple supporting factors. First, we

510 propose that there is a possible lithological bedrock control. The northern shoreline is dominated by

511 Globigerina Marls (Helvetic nappes) and in the south by Flysch (Helvetic n.), dolomite, gypsum and

512 clays (Triassic and Penninic n.). These bedrock types are rather sensitive to erosion and can be easily

513 removed by the erosional power of subglacial meltwater.

514 Secondly, there is a tectonic control via Hohgant-Sundlauenen fault (Fig. 6) that caused a

515 synsedimentary extensional movement (Breitschmid, 1978) with a displacement of up to 1025 m in

516 Cretaceous-Eocene times (Häuselmann, 2002) and provides a weak zone supporting the creation of

517 the overdeepened basin. A prolongation of the fault into Lake Thun is very likely and depicted in Fig.

518 6. The bedrock elevation drop in the lake at the presumed continuation of the fault amounts to 240 m.

519 These observations suggest that the overdeepening was caused by a combination of subglacial

520 erosional processes and tectonic predisposition (Preusser et al., 2010; Dürst Stucki and Schlunegger,

521 2013). Towards the NW, bedrock rises to higher elevations: at the drilling site Thalgut, 10 km NNW

522 of Thun outside the lake, bedrock was encountered at 147 m below surface. Figs. 3 and 6 illustrate

523 this continuously rising bedrock surface from the deepest point of the basin towards the outlet. Reber

524 and Schlunegger (2016) calculated the thickness of Quaternary sediments of 100–150 m underneath

525 the city of Thun. According to their model, bedrock then stays at fairly constant elevation with a slight

526 descent towards Bern. From the deepest basin towards Interlaken, bedrock rises steeply at ~26° and

527 peaks at 200 m below surface, building a barrier that hosts the platform and the subaquatic moraine.

528 **4.2. Timing of glacial deposition (till 1 to 3)**

529 The time of emplacement of the thick glacial deposits (U1–U3) can only be done in a qualitative way,

530 since there is no deep drill core data available from Lake Thun for temporal classification. U3 is the

531 youngest glacial unit and covers the entire basin, therefore we attribute it to LGM. The older

532 sequences U1 and U2 cannot be put into temporal context with the data at hand. Generally, two

533 plausible scenarios can be imagined:

534 1) A multi-cycle concept, where U1 and U2 belong to independent pre-LGM glacial cycles, as it is

535 documented for the Aare valley at nearby drill site Thalgut (Schlüchter, 1989a; 1989b; see Fig. 10 for

536 location) or known from the drill site at Lake Zurich (Lister et al., 1984) with four till sequences that

537 are all topped by glacio-lacustrine sediments deposited in a lacustrine (subglacial) environment. Also

538 Lake Annecy and Lake Le Bourget, France, host remnants of pre-LGM sediments (Van Rensbergen et

539 al., 1998; van Rensbergen et al., 1999). U1 and U2 most likely postdate the mid-Pleistocene, since

540 Häuselmann et al. (2008) unraveled evidence for five glacial advances in the Aare valley within the

541 last ~220ka based on dated speleothems.

542 2) A multi-phase single cycle concept, where U1 and U2 are part of the last glaciation. Fiord-type

543 lakes in British Columbia, Canada, and the New York Finger Lakes show that sediments predating the

544 last glacial cycle must have been entirely eroded and only massive diamicts of several hundred meters

545 thickness witness the last glacial cycle (Eyles et al., 1991; Mullins et al., 1996; Eyles and Mullins,

546 1997).

547 While U3 signals a grounded glacier, which eventually starts to lift off the ground, retreat and

548 disintegrate, U4 was deposited temporally between the abandonment of the LGM position and the halt

549 of the glacier to form a "quasi-stagnant", slightly fluctuating ice front at Interlaken. Since U4 is

550 restricted to the deepest basin, a subglacial lake developed most likely within this short time frame,

551 with subglacial meltwater and glacier melt-out providing most of the glacio-lacustrine sedimentary

552 input. The rapid disintegration and readvance left no time for a basin-wide deposition of lacustrine

553 sediments.

554

555

556

4.3. Depositional concept of the Sundlauenen subaquatic moraine complex (SMC)

The interpretation of Fig. 5 can be approached in two different ways:

SMC Model 1

The conceptual model created by Lønne (1995) for ice-contact submarine fan systems and the corresponding ice-front advance-retreat (mini-)cycles — we introduce here the term mini-cycle to avoid confusion with major glacial cycles — applies also to glacio-lacustrine environments. These systems often show a slow advance phase, a short stillstand of the glacial front, followed by a rapid disintegration (Meier and Post, 1987; Lønne and Nemec, 2011). One complete mini-cycle holds five allostratigraphic units, defined on the basis of outcrops, seismic sections and ground-penetrating radar, which they then applied to temperate glaciers in Norway (Lønne, 1995; Lønne and Syvitski, 1997; Lønne, 2001; Lønne and Nemec, 2011). We slightly adopted their scheme to three allostratigraphic units to fit best with our observations. The subscript "L" stands for "Lønne" to avoid confusion with nomenclature used in this study. They list the units of a mini-cycle in a seismic or outcrop section as follows from bottom to top:

A_L ice-contact facies during glacier advance (foresets coarsening upfan, bottomsets intercalated by sandy turbidites, including syn-sedimentary glacio-tectonic deformation, erosion)

B_L ice-contact facies during glacier stillstand/retreat (foreset beds, bottom set beds, boundary A_L/B_L erosive in the upper part and concordant towards the bottom sets, deformation/erosion on ice-proximal slope possible)

C_L ice-distal facies formed during retreat (sediment from meltwater deposited over entire ridge, no deformation)

A_L-B_L-C_L resembling one glacial mini-cycle are partly relatable to the Sundlauenen subaquatic moraine in Fig. 5. To be most in accordance with the scheme introduced by Lønne (1995) and Lønne and Syvitski (1997), subunits 1 A/B to subunits 4 A/B would all belong to a phase A_L, ice-contact facies formed during glacial (re)advance. This is mainly based on the forestepping character of the subunits A with respect to each other. After 1A/B to 4A/B, it follows a period of glacial stillstands and or slight retreats with subunits 5A/B to 7A/B mainly based on the thick accumulation of 5A, 6A and 7A on the ice-proximal slope and the relative location of the crests to previously deposited material indicating backstepping. Allostratigraphic unit C_L is not recognizable, either because most of it has been reworked and used in the subsequent readvance, or the thickness of the subunit is beyond the resolution of the seismic data. This second part of the mini-cycle is terminated by 8A, what is called Bt_L and interpreted as basal ice-contact facies, showing the last retreating stage and the final abandonment with the *termination* of the mini-cycle. This is followed by the deposition of unit C_L,

590   ice-distal sediments signaling the final retreating stage, represented by the base of units U6 and U9 (in

591   summary the mini-cycle would be A_L-A_L-A_L-A_L-B_L-B_L-B_L-Bt_L-C_L).

592   *SMC Model 2*

593   A different approach would be to tie each single depositional package made of subunits A & B as a

594   readvance that might be followed by a short phase of stillstand (Fig. 8A). Readvance/stillstand were

595   not necessarily always interrupted by a retreating phase, since a stillstand can be directly followed by

596   a renewed advance. However, the clear separation of individual packages, including the fact that

597   foresets and bottom sets of single packages show a low-amplitude base and reveal clearer high-

598   amplitude reflections towards the top (Fig. 5), suggests that the sediment emplacement was not

599   continuous throughout time. It was relatively more significant at the onset of deposition and ceasing

600   with time until an interruption occurred during short phases of smaller or larger retreats accompanied

601   by sediment dumping to the proglacial area (Fig. 8B). The sediment dumping occurs likely in the

602   form of turbiditic events in the proximal slope area. The bottom set beds most likely contain

603   intercalated mass-movement related turbidites and fluvial input from tributaries, as the sudden glacial

604   retreat promotes slope instabilities. Any moraine material deposited at the top of the ridge or in the

605   proglacial area during a readvance of the glacier is eventually overrun and partially eroded,

606   remobilized and reused to form a new crest during a subsequent readvance (Fig. 8C). Hence, what we

607   observed are rather pulses of readvances, occasionally interrupted by short retreats with no deposition

608   (Lønne and Nemec, 2011), resembled by every single package rather than a continuous succession of

609   deposits through time. Therefore, every single package could reflect a short (re)advance-retreat mini-

610   cycle, totaling to seven such cycles. Eventually, climatic conditions change and final abandonment of

611   the stadial position takes place with ice-distal sedimentation primarily at the ice-proximal slope side

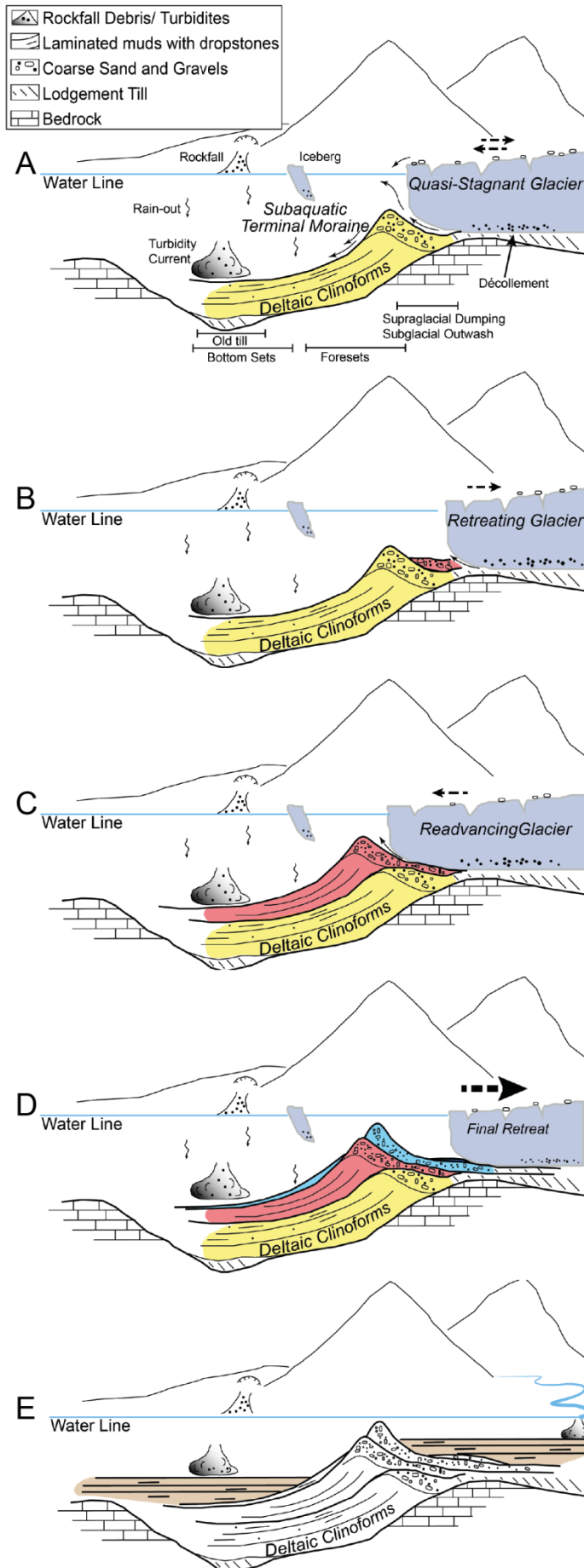612   of the crest (Fig. 8D,E).

613

Fig. 8: Conceptual model illustrating the relative chronology of the recessional phase of the Aare Glacier. A) Stagnant or slightly readvancing phase. B) Retreating phase. C) Readvancing phase and moraine and deltaic clinoform build-up. Previous moraine crest is overridden and partially eroded. D) Rapid retreat. E) Complete abandonment of stadial position. Glacio-lacustrine, but mainly lacustrine and fluvial sedimentation dominate.

614

615 It is important to note that the stratigraphic thickness of the bottom sets is to some extent correlated to
616 the thickness of the till placed at the top of the crest. E.g. 1A) in Fig. 5 shows a thick deposit of till
617 and hence also a thick sequence of bottom sets. 4A) is almost non-existent and hence there is hardly
618 any bottom sets distinguishable that can be assigned to 4B).

619 *Combination of SMC Models 1 & 2*

620 Fig. 9 summarizes the two presented conceptual models above based on measurements taken from
621 seismic sections 09 and 20. Fig. 9 (left panel) shows the reconstructed ice-front movements, based on
622 the positions of individual moraine crests in U5 of line 20. The location of the subaquatic grounded
623 glacial front is picked at the location of the peak of each crest. The cumulative bottom set thickness
624 was measured in the deepest basin of line 20. Subunits 1–4 show a prograding system with each new
625 moraine crest being placed further downstream, formed by an advancing glacier that overruns
626 previous deposits. Single subunits are well distinguishable in seismic data, suggesting a stagnant
627 period of the glacier towards the end of an advancing phase, which is possibly followed by a short
628 retreat (Fig. 9 grey dotted lines) before the initiation of a readvance. Subunits 5–7 show an
629 aggrading/retrograding system with crest formation mainly during a stagnant phase or shortly after a
630 small retreat followed by a readvance.

631 The dip angles of the foresets are measured on line 09, since the orientation of the line is
632 perpendicular to the strike direction of the SMC (Fig. 5 inset). Line 20 displays apparent dips which
633 differ from the true values measured on line 09. The right panel in Fig. 9 shows that dip angles
634 steepen during the build-up of the complex (subunits 1–4) and start to decline thereafter (subunits 5–
635 7). Similarly, the bottom set thickness increases during build-up and starts to cease in the
636 aggrading/retrograding phase. Subunit 4 shows the steepest foresets, but no bottom set deposits are
637 recognizable due to the limited resolution in the seismic data set or a phase of almost no deposition in
638 the deep basin, indicating a dramatic change in accommodation space (forestepping to backstepping)
639 leading to sediment starvation in the basin.

640
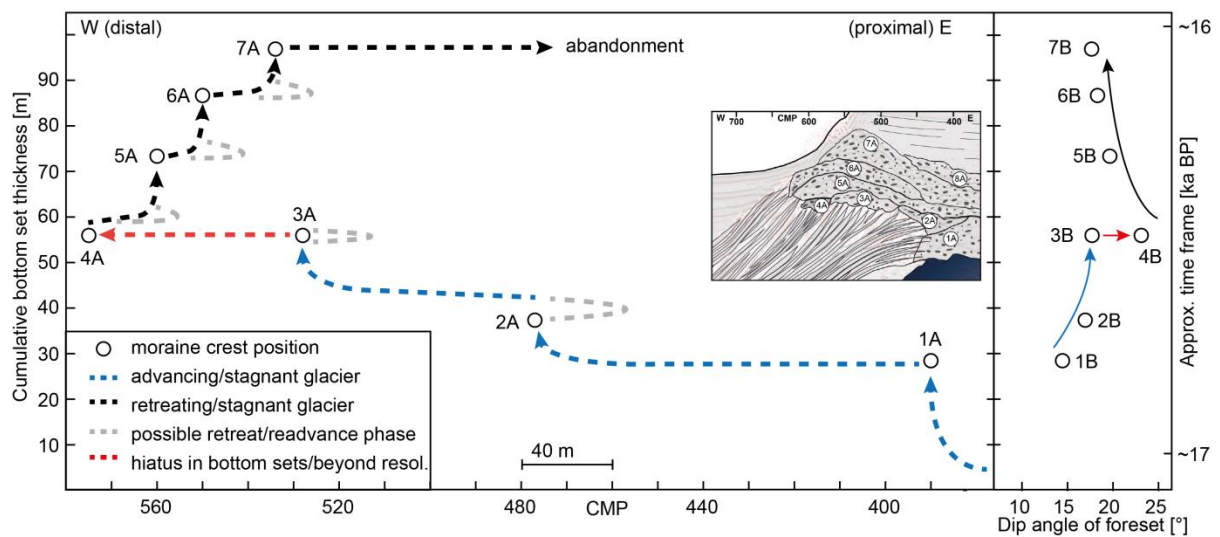
Fig. 9: Left panel: Ice-front movements based on moraine crest positions in U5 of line 20 (see extract

from Fig. 5), plotted versus cumulative bottom set thickness taken at CMP 1600 in line 20. Right

panel: Right panel: Dip angles taken close to the moraine crests at the steep onset of the forests in

line 09. Median of 10 measurements is plotted with a standard error smaller than the circle size.

Steepening of the angles during overall glacial advance and flattening during overall retreat.

Hence, the thickness of the bottom sets is related to the sediment productivity of the system, which is

a function of time, sediment availability and efficiency in sediment mobilization (sub-, supra-, en- and

proglacially). The controls on accommodation space and the depositional pattern are not so much

driven by changes in relative lake level or tectonic movements, as it is the case in a typical marine

setting (e.g. Catuneanu et al., 2011), but are rather tied to the behavior of the ice front (single pulses

of advance, stillstand, retreat), which cause forestepping, upstepping and backstepping. The bottom

set beds of U5 represent almost 1/5 of the entire infill thickness (~ 550 m), indicating high

sedimentation rates, followed by a rapid disintegration, which may be even comparable to the down-

wasting observed since the end of the 20th century (Paul et al., 2007).

The material for the build-up of the SMC is provided by two sources: subglacial diamict material

from the deforming layer the glacier sits on and/or basal till and outwash material from meltwater

outflow (Lønne, 1995). Apart from the re-mobilization of subglacial material and proglacial

sediments along a basal gliding plane (décollement), the complex might be additionally promoted by

ice-marginal glacial dumping, glacial thrusting (thrust faults in Fig. 5 bottom) and meltout (Bennett

and Glasser, 2009). Whatever process dominated the build-up, the formation of the SMC was

involved a number of different processes.

4.4. Deglaciation

The deglaciation history of the Aare valley since the Last Glacial Maximum is constrained by a

limited set of absolute ages illustrated in Fig. 10. Akcar et al. (2011) dated an erratic boulder to 19 ±

665   0.9 ka at Möschberg (T1 in Fig. 10) applying cosmogenic nuclide surface-exposure dating (erosion-

666   corrected [10]Be age). At least until this time, the Aare valley was covered by a thick valley glacier.

667   Wirsig et al. (2016) obtained a robust minimum exposure age of 17.7 ± 0.8 ka for the onset of the

668   deglaciation. The timing of ice-free conditions is given by the radiocarbon-dated calcareous clay

669   gyttja from 8.3 m depth in Late-Glacial Lake Amsoldingen, located adjacent to the water outlet of

670   Lake Thun. It shows an age of ~16.3 ka BP (Lotter, 1985), providing a minimum age for an ice-free

671   area at the small lake (T2 in Fig. 10).

672   Furthermore, the Late-Glacial retreat of the Aare Glacier into its high-Alpine catchment upstream of

673   Lake Thun was investigated by Wirsig et al. (2016). They modelled the Aare Glacier ice extent

674   combining glacial striae, trimline elevations with surface exposure ages and GIS ice surface models.

675   Their most conservative model for the Gschnitz stadial resulted in a terminal position of the Aare

676   Glacier as far downstream as Interlaken between Lake Brienz and Lake Thun. However, models with

677   less shear stress on the bed agrees better with their observed striae and elevation patterns suggesting a

678   terminal position at Innertkirchen between 17–16 ka (T4 in Fig. 10), which might represent the

679   Gschnitz stadial (Wirsig et al., 2016, recalculated from Ivy-Ochs et al., 2006). On the basis of [10]Be

680   exposure ages of boulders from the end moraine at the type locality at Trins (Austria), Ivy-Ochs et al.

681   (2006) dated the Gschnitz stadial to 15.4 ka ± 1.4 ka. Glacial readvance was initiated about 500 years

682   earlier and is expected to emplace significant moraine crests, which to date are missing, hidden or not

683   preserved for many larger glaciers such as the Aare Glacier. In the Aare valley, the end position for

684   the next younger stadial, the Egesen stadial at 12.9–11.5 ka (T5 in Fig. 10, Wirsig et al., 2016) lies

685   between Handegg and Guttannen.

686   Neither model by Wirsig et al. (2016), with T4 at Interlaken or at Innertkirchen can explain the

687   obtained scatter in exposure ages (13.6–16.1 ka) from boulders and bedrock samples at a local

688   through shoulder at a high-altitude site (Gelmerhörner ridge). Currently, Wirsig et al. (2016) assume a

689   local remaining ice patch has covered the ridge during Gschnitz stadial or toppling and spalling leads

690   to the scatter. Alternatively, this might be tackled with a model suggesting a terminal moraine position

691   beyond Interlaken (e.g. at T3), causing an elevated ice coverage to an altitude that is in better

692   agreement with the observed [10]Be ages at Gelmerhörnli.

693

694
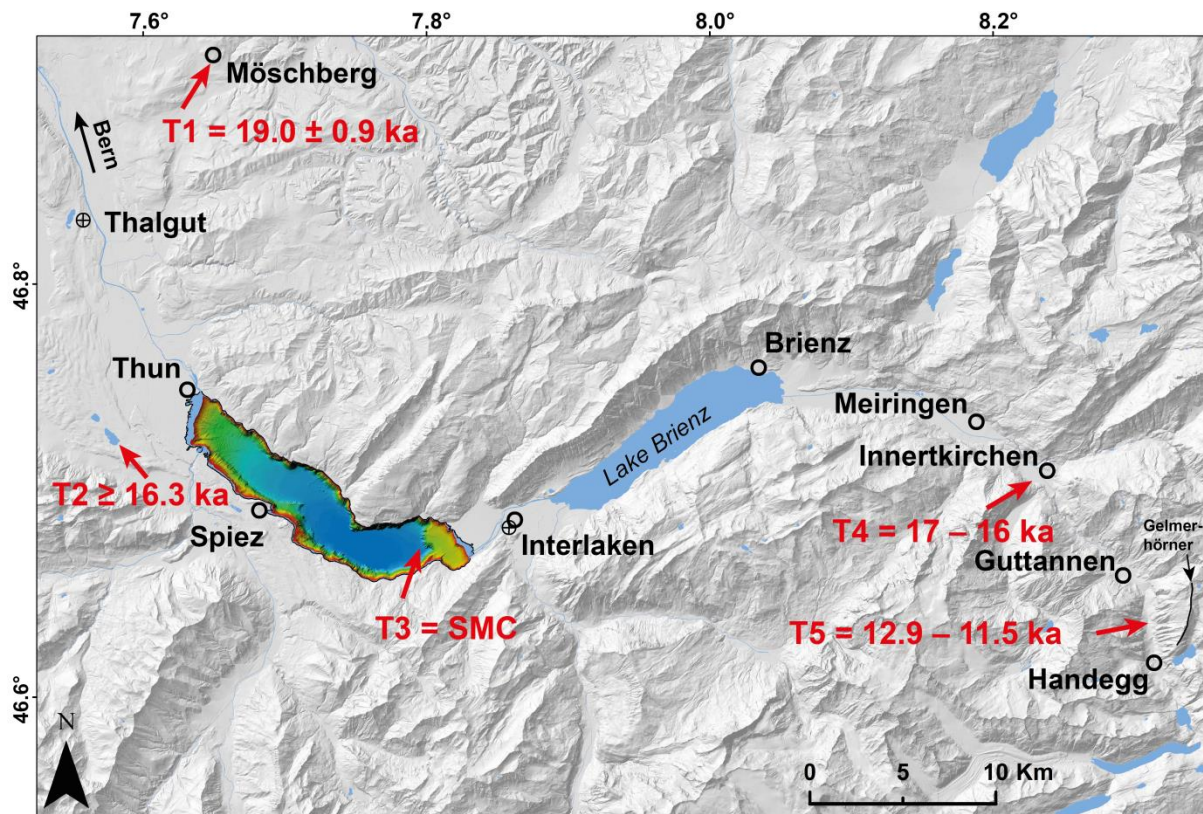
Fig. 10: Overview of available age constraints regarding the deglaciation stages of the Aare Glacier

between LGM and the Younger Dryas. The crossed circles indicate drilling sites Thalgut and

Interlaken Hospital. See text for more details.

698 The time window for the Aare Glacier to retreat from T1 to T5 amounts thus to ~5,200 – 8,400 ka.

699 The calibrated radiocarbon age (using IntCal13, Reimer et al., 2013) of T2 of ~16.3 ± 0.3 ka cal BP

700 age (uncalibrated ^{14}C-age 13.49 ka ± 0.17, calibrated 2-sigma range is 16,801–15,769 years BP, Lotter

701 et al., 1985) gives rather a lower bound and is most likely underestimating the age. But assuming the

702 onset of the deglaciation of the Aare valley occurred no later than 17.7 ka, the available time window

703 for the glacier tongue to recede ~80 km from Bern (17.7 ± 0.8 ka) all the way upstream to

704 Innertkirchen (T4, 16.5 ± 1.4, dating error from Ivy-Ochs et al., 2006) amounts to 1.2 ± 1.6 ka. Hence

705 the time window for the formation of the SMC narrows to less than 1,000 years. This suggests that the

706 Aare Glacier disintegrated rapidly, similar to the fast ice-collapse of the Garda glacial amphitheater as

707 proposed by Ravazzi et al. (2014), and was accompanied by extraordinary high sedimentation rates.

708 The combined thickness of U4 and U5 (Fig. 7E) amounts to ~175 ± 10 m in the deepest basin,

709 accumulated between the abandonment of the Aare Glacier's LGM position (19.0 ± 0.9 ka) and the

710 position at Innertkirchen (16.5 ± 1.4 ka). This conservative estimation leads to a sedimentation rate of

711 7.0 ± 0.7 cm/yr. If we consider U5 separately, apply the assumption above and take into the

712 calculation ~100 ± 5 m of bottom set sediments deposited in less than 1.2 ± 1.6 ka, we obtain a

713 sedimentation rate of >8.3 ± 1.3 cm/yr during SMC formation. This seems a reasonable estimate for a

714 rapidly disintegrating Aare Glacier, as the sedimentation rate in Lake Zurich immediately after glacial

31

715 withdrawal ~17 ka ago was calculated to be ~11 cm/yr (Lister et al., 1984). However, better time
716 constraints could possibly result in a sedimentation rate even twice as high.

5. Summary and conclusions

718 Using the combination of multibeam bathymetry data and multi-channel reflection seismic data, we
719 present a new bedrock map of the Lake Thun basin, highlighting the importance of an accurate
720 velocity model in order to obtain correct depth values. The overdeepened bedrock incision reaching
721 770 m below today's lake surface or down to ~220 m below current sea level is in agreement with
722 other perialpine lakes. Bedrock incision is the result of a combination of forces primarily represented
723 by subglacial meltwater and glacial scouring. It was additionally promoted by stratigraphic and
724 tectonic predisposition providing erosion-prone bedrock formations and pre-existing deformation
725 features, such as the Hohgant-Sundlauenen fault.

726 The multi-channel reflection seismic data allowed a detailed seismic stratigraphic analysis. Ten units
727 (U0–U9) have been identified. The uppermost waterlain till (U3) belongs to the last glaciation.
728 Underlying till units (U1, U2) are either part of the last glaciation and signal changes in the
729 depositional environment (multi-phase single cycle) or, more likely, represent independent remains of
730 pre-LGM glacial cycles. The subsequent unit U5 illustrates an intermediate halt during a dramatic
731 recessional phase of the Aare Glacier. The detailed seismic stratigraphic analysis revealed a to-date
732 unknown subaquatic moraine complex and its internal architecture in the Lake Thun basin. Its eight
733 subunits are distinct individual depositional packages indicating local fluctuation of the ice front with
734 single pulses of advance and retreat distinguishable.

735 The two presented conceptual models for the build-up of the Sundlauenen subaquatic moraine
736 complex (SMC) represent two end-member scenarios. A combination of the two models that allows
737 for individual (re)advance-retreat mini-cycles, despite the systematic lack of deposits signaling clear
738 retreats due to re-mobilization of material, seems to fit best with our findings from the stratigraphic
739 analysis. Existing age constraints indicate that the retreat of the Aare Glacier to its inner-Alpine
740 region and the formation of the SMC occurred in less than 1,000 years, accompanied by
741 sedimentation rates exceeding 8 cm/yr.

742 Further investigations are needed to constrain the timing of the deposition of the Sundlauenen
743 subaquatic moraine complex within the Late-Glacial stratigraphy. Namely, whether the SMC can be
744 correlated with stadial climatic deteriorations, e.g. the Gschnitz stadial that has been so far lacking in
745 the major longitudinal valleys within the Alps, or it has to be considered as an exceptional occurrence
746 that signals a so far unknown perturbation in an almost traceless deglaciation history.

747

Competing interest

The authors declare that they have no conflict of interest.

Acknowledgements

References

Akcar, N., Ivy-Ochs, S., Kubik, P. W., and Schluchter, C., (2011) Post-depositional impacts on 'Findlinge' (erratic boulders) and their implications for surface-exposure dating. *Swiss Journal of Geosciences*, 104(3), p. 445-453.

Anselmetti, F. S., Drescher-Schneider, R., Furrer, H., Graf, H. R., Lowick, S. E., Preusser, F., and Riedi, M. A., (2010) A similar to 180,000 years sedimentation history of a perialpine overdeepened glacial trough (Wehntal, N-Switzerland). *Swiss Journal of Geosciences*, 103(3), p. 345-361.

Beck, P., (1907) Der diluviale Bergsturz von St. Beatenberg. *Mitteilungen der Naturforschenden Gesellschaft in Bern*.

Beck, P., (1920-1922) Grundzüge der Talbildung im Berner Oberland. *Eclogae Geologicae Helvetiae*, 16(2), p. 39.

Beck, P., (1933) Über das schweizerische und europäische Pliozän und Pleistozän. *Eclogae Geologicae Helvetiae*, 26(2), p. 335-437.

Bennett, M. R., (2001) The morphology, structural evolution and significance of push moraines. *Earth-Science Reviews*, 53(3), p. 197-236.

Bennett, M. R., and Glasser, N. F., 2009, Glacial Geology: Ice Sheet and Landforms, Wiley-Blackwell.

Bini, A., Buoncristiani, J.-F., Couterrand, S., Ellwanger, D., Felber, M., Florineth, D., Graf, H. R., Keller, O., Kelly, M., Schlüchter, C., and Schoeneich, P., (2009) Switzerland during the Last Glacial Maximum 1: 500'000. *Bundesamt für Landestopografie swisstopo.*

Bini, A., Cita, M. B., and Gaetani, M., (1978) Southern Alpine lakes — Hypothesis of an erosional origin related to the Messinian entrenchment. *Marine Geology*, 27(3), p. 271-288.

Bodmer, R., Matter, A., and Scheller, E., (1973) Geologische, seismische und pollenanalytische Untersuchung im Bödeli bei Interlaken. *Mitteilungen der Naturforschenden Gesellschaft in Bern*, 30), p. 14.

787   Boulton, G. S., Dobbie, K. E., and Zatsepin, S., (2001) Sediment deformation beneath
788   glaciers and its coupling to the subglacial hydraulic system. *Quaternary International*,
789   86), p. 3-28.
790   Bouma, A. H., (1987) Megaturbidite - an Acceptable Term. *Geo-Marine Letters*, 7(2), p. 63-
791   67.
792   Breitschmid, A., (1978) Sedimentologische Untersuchungen in der eocaenen Hohgant-Serie
793   im Helvetikum nördlich von Interlaken. *Eclogae Geologicae Helvetiae*, 71), p. 143-
794   157.
795   Buechi, M. W., Frank, S. M., Graf, H. R., Menzies, J., and Anselmetti, F. S., (2017)
796   Subglacial emplacement of tills and meltwater deposits at the base of overdeepened
797   bedrock troughs. *Sedimentology*, 64(3), p. 658-685.
798   Catuneanu, O., Galloway, W. E., Kendall, C. G. S., Miall, A. D., Posamentier, H. W.,
799   Strasser, A., and Tucker, M. E., (2011) Sequence Stratigraphy: Methodology and
800   Nomenclature. *Newsletters on Stratigraphy*, 44(3), p. 173-245.
801   Chopra, S., Castagna, J., and Portniaguine, O., (2006) Seismic resolution and thin-bed
802   reflectivity inversion. *CSEG recorder*, 31(1), p. 19-25.
803   Clark, P. U., Dyke, A. S., Shakun, J. D., Carlson, A. E., Clark, J., Wohlfarth, B., Mitrovica, J.
804   X., Hostetler, S. W., and McCabe, A. M., (2009) The Last Glacial Maximum.
805   *Science*, 325(5941), p. 710-714.
806   Dehnert, A., Lowick, S. E., Preusser, F., Anselmetti, F. S., Drescher-Schneider, R., Graf, H.
807   R., Heller, F., Horstmeyer, H., Kemna, H. A., Nowaczyk, N. R., Zuger, A., and
808   Furrer, H., (2012) Evolution of an overdeepened trough in the northern Alpine
809   Foreland at Niederweningen, Switzerland. *Quaternary Science Reviews*, 34), p. 127-
810   145.
811   Dürst Stucki, M., and Schlunegger, F., (2013) Identification of erosional mechanisms during
812   past glaciations based on a bedrock surface model of the central European Alps. *Earth
813   and Planetary Science Letters*, 384), p. 57-70.
814   Ehlers, J., and Gibbard, P. L., 2004, Quaternary glaciations-extent and chronology: part I:
815   Europe, Elsevier.
816   Escher, H. C., (1820) Über die fremdartigen Geschiebe und Felsblöcke, welche sich in
817   verschiedenen Ländern vorfinden, mit Hinsicht auf Herrn J.A. De Luc's des Jüngern
818   in Genf hierüber aufgestellten Hypothese. *Annalen der Physik*, 65(5), p. 15
819   Eyles, N., and Mullins, H. T., (1997) Seismic-stratigraphy of Shuswap Lake, British
820   Columbia, Canada. *Sedimentary Geology*, 109(3), p. 283-303.
821   Eyles, N., Mullins, H. T., and Hine, A. C., (1991) The seismic stratigraphy of Okanagan
822   Lake, British Columbia; a record of rapid deglaciation in a deep 'fiord-lake' basin.
823   *Sedimentary Geology*, 73(1), p. 13-41.
824   Fanetti, D., Anselmetti, F. S., Chapron, E., Sturm, M., and Vezzoli, L., (2008) Megaturbidite
825   deposits in the Holocene basin fill of Lake Como (Southern Alps, Italy).
826   *Palaeogeography Palaeoclimatology Palaeoecology*, 259(2-3), p. 323-340.
827   Fiebig, M., Herbst, P., Drescher-Schneider, R., Luthgens, C., Lomax, J., and Doppler, G.,
828   (2014) Some remarks about a new Last Glacial record from the western Salzach
829   foreland glacier basin (Southern Germany). *Quaternary International*, 328), p. 107-
830   119.
831   Finckh, P., Kelts, K., and Lambert, A., (1984) Seismic Stratigraphy and Bedrock Forms in
832   Perialpine Lakes. *Geological Society of America Bulletin*, 95(9), p. 1118-1128.
833   Finckh, P. G., (1978) Are southern Alpine lakes former Messinian canyons? — Geophysical
834   evidence for preglacial erosion in the southern Alpine lakes. *Marine Geology*, 27(3),
835   p. 289-302.

836 Fiore, J., Girardclos, S., Pugin, A., Gorin, G., and Wildi, W., (2011) Wurmian deglaciation of
837   western Lake Geneva (Switzerland) based on seismic stratigraphy. *Quaternary*
838   *Science Reviews*, 30(3-4), p. 377-393.
839 Fiore, J. T., 2007, Quaternary subglacial processes in Switzerland: Geomorphology of the
840   Plateau and seismic stratigraphy of Western Lake Geneva: University of Geneva.
841 Giovanoli, F., Kelts, K., Finckh, P., and Hsü, J., (1984) Geological framework, site survey
842   and seismic stratigraphy In: Quaternary geology of Lake Zurich: An interdisciplinary
843   investigation by deep-lake drilling. *Contributions to Sedimentology*, 13), p. 5-20.
844 Haeuselmann, P., Granger, D. E., Jeannin, P. Y., and Lauritzen, S. E., (2007) Abrupt glacial
845   valley incision at 0.8 Ma dated from cave deposits in Switzerland. *Geology*, 35(2), p.
846   143-146.
847 Häuselmann, P., 2002, Cave Genesis and its relationship to surface processes: Investigation
848   in the Siebenhengste region (BE, Switzerland) [PhD Dissertation]: University
849   Freiburg (Switzerland), 170 p.
850 Häuselmann, P., Lauritzen, S. E., Jeannin, P. Y., and Monbaron, M., (2008) Glacier advances
851   during the last 400 ka as evidenced in St. Beatus Caves (BE, Switzerland).
852   *Quaternary International*, 189), p. 173-189.
853 Heim, A., (1894) Ueber das absolute Alter der Eiszeit. *Vierteljahrsschrift der*
854   *Naturforschenden Gesellschaft in Zürich*, 39), p. 180-186.
855 Hilbe, M., and Anselmetti, F. S., (2014) Signatures of slope failures and river-delta collapses
856   in a perialpine lake (Lake Lucerne, Switzerland). *Sedimentology*, 61(7), p. 1883-1907.
857 Hilbe, M., Anselmetti, F. S., Eilertsen, R. S., Hansen, L., and Wildi, W., (2011) Subaqueous
858   morphology of Lake Lucerne (Central Switzerland): implications for mass
859   movements and glacial history. *Swiss Journal of Geosciences*, 104(3), p. 425-443.
860 Hinz, K., Richter, I., and Sieber, N. P., (1970) Reflexionsseismische Untersuchungen im
861   Zürichsee. Teil 1: Geophysik. *Eclogae Geologicae Helvetiae*, 63(2), p. 511-523.
862 Hughes, P. D., Gibbard, P. L., and Ehlers, J., (2013) Timing of glaciation during the last
863   glacial cycle: evaluating the concept of a global 'Last Glacial Maximum' (LGM).
864   *Earth-Science Reviews*, 125), p. 171-198.
865 Ivy-Ochs, S., (2015) Glacier Variations in the European Alps at the End of the Last
866   Glaciation. *Cuadernos De Investigacion Geografica*, 41(2), p. 295-315.
867 Ivy-Ochs, S., Kerschner, H., Kubik, P. W., and Schlüchter, C., (2006) Glacier response in the
868   European Alps to Heinrich Event 1 cooling: the Gschnitz stadial. *Journal of*
869   *Quaternary Science*, 21(2), p. 115-130.
870 Ivy-Ochs, S., and Kober, F., (2008) Surface exposure dating with cosmogenic nuclides.
871   *Quaternary Science Journal*, 57(1-2), p. 179-209.
872 Ivy-Ochs, S., Schafer, J., Kubik, P. W., Synal, H. A., and Schluchter, C., (2004) Timing of
873   deglaciation on the northern Alpine foreland (Switzerland). *Eclogae Geologicae*
874   *Helvetiae*, 97(1), p. 47-55.
875 Jäckli, H., (1962) Die Vergletscherung der Schweiz im Würmmaximum. *Eclogae Geologicae*
876   *Helvetiae*, 55(2), p. 285-294.
877 Johnson, M. D., Benediktsson, I. O., and Bjorklund, L., (2013) The Ledsjo end moraine-a
878   subaquatic push moraine composed of glaciomarine clay in central Sweden.
879   *Proceedings of the Geologists Association*, 124(5), p. 738-752.
880 Kelly, M. A., Ivy-Ochs, S., Kubik, P. W., von Blanckenburg, F., and Schluchter, C., (2006)
881   Chronology of deglaciation based on Be-10 dates of glacial erosional features in the
882   Grimsel Pass region, central Swiss Alps. *Boreas*, 35(4), p. 634-643.
883 Kerschner, H., Ivy-Ochs, S., and Schluchter, C., (1999) Paleoclimatic interpretation of the
884   early Late-glacial glacier in the Gschnitz valley, central Alps, Austria. *Annals of*
885   *Glaciology, Vol 28*, 28), p. 135-140.

886   Kremer, K., Simpson, G., and Girardclos, S., (2012) Giant Lake Geneva tsunami in AD 563.
887   *Nature Geosci*, 5(11), p. 756-757.
888   Lister, G. S., Giovanoli, F., Eberli, G., Finckh, P., Finger, W., He, Q., Heim, C., Hsu, K. J.,
889   Kelts, K., Peng, C., Sidler, C., and Zhao, X., (1984) Late Quaternary Sediments in
890   Lake Zurich, Switzerland. *Environmental Geology*, 5(4), p. 191-205.
891   Lønne, I., (1995) Sedimentary Facies and Depositional Architecture of Ice-Contact
892   Glaciomarine Systems. *Sedimentary Geology*, 98(1-4), p. 13-43.
893   Lønne, I., (2001) Dynamics of marine glacier termini read from moraine architecture.
894   *Geology*, 29(3), p. 199-202.
895   Lønne, I., and Nemec, W., (2011) Modes of sediment delivery to the grounding line of a fast-
896   flowing tidewater glacier: implications for ice-margin conditions and glacier
897   dynamics. *Ice-Marginal and Periglacial Processes and Sediments*, 354), p. 33-56.
898   Lønne, I., and Syvitski, J. P., (1997) Effects of the readvance of an ice margin on the seismic
899   character of the underlying sediment. *Marine Geology*, 143(1-4), p. 81-102.
900   Lotter, A. F., (1985) Amsoldingersee-Late glacial and Holocene environments of a lake at the
901   southern edge of the Swiss plateau. *Dissertation Botanicae*, 87), p. 185-208.
902   Matter, A., Dessolin, D., Sturm, M., and Süsstrunk, A. E., (1973) Reflexionsseismische
903   Untersuchung des Brienzersees. *Eclogae Geologicae Helvetiae*, 66), p. 71-82.
904   Matter, A., Suesstrunk, A. E., Hinz, K., and Sturm, A., (1971) Ergebnisse
905   reflexionsseismischer Untersuchungen im Thunersee. *Eclogae Geologicae Helvetiae*,
906   64(3), p. 505-520.
907   Meier, M. F., and Post, A., (1987) Fast Tidewater Glaciers. *Journal of Geophysical
908   Research-Solid Earth and Planets*, 92(B9), p. 9051-9058.
909   Menzies, J., and Shilts, B. W., (2002), 8 - Subglacial environments. *Modern and Past
910   Glacial Environments,* p. 183-278.
911   Mix, A. C., Bard, E., and Schneider, R., (2001) Environmental processes of the ice age: land,
912   oceans, glaciers (EPILOG). *Quaternary Science Reviews*, 20(4), p. 627-657.
913   Monegato, G., Scardia, G., Hajdas, I., Rizzini, F., and Piccin, A., (2017) The Alpine LGM in
914   the boreal ice-sheets game. *Scientific Reports*, 7(1), p. 2078.
915   Muir-Wood, R., (1989), Extraordinary Deglaciation Reverse Faulting in Northern
916   Fennoscandia. *Earthquakes at North-Atlantic Passive Margins: Neotectonics and
917   Postglacial Rebound,* p. 141-173.
918   Muir-Wood, R., (2000) Deglaciation Seismotectonics: a principal influence on intraplate
919   seismogenesis at high latitudes. *Quaternary Science Reviews*, 19(14), p. 1399-1411.
920   Mullins, H. T. Eyles, N., Mullins, H. T., Hinchey, E. J., Wellner, R. W., Stephens, D. B.,
921   Anderson, J. W. T., Dwyer, T. R., and Hine, A. C., (1996), Seismic stratigraphy of the
922   Finger Lakes: A continental record of Heinrich event H-1 and Laurentide ice sheet
923   instability. *Subsurface geologic investigations of New York Finger Lakes:
924   implications for late Quaternary deglaciation and environmental change*.
925   Ndiaye, M., Clerc, N., Gorin, G., Girardclos, S., and Fiore, J., (2014) Lake Neuchatel
926   (Switzerland) seismic stratigraphic record points to the simultaneous Wurmian
927   deglaciation of the Rhone Glacier and Jura Ice Cap. *Quaternary Science Reviews*, 85),
928   p. 1-19.
929   Paul, F., Kaab, A., and Haeberli, W., (2007) Recent glacier changes in the Alps observed by
930   satellite: Consequences for future monitoring strategies. *Global and Planetary
931   Change*, 56(1-2), p. 111-122.
932   Penck, A., (1905) Glacial Features of the Surface of the Alps. *Geographical Teacher*, 3(2), p.
933   49-61.
934   Penck, A., and Brückner, E., (1909) Die Alpen im Eiszeitalter. Zweiter Band: Die Eiszeiten
935   in den nördlichen Westalpen. *Leipzig: C.H. Tauschnitz*.

936   Piotrowski, J. A., Mickelson, D. M., Tulaczyk, S., Krzyszkowski, D., and Junge, F. W.,
937   (2001) Were deforming subglacial beds beneath past ice sheets really widespread?
938   *Quaternary International*, 86), p. 139-150.
939   Preusser, F., Drescher-Schneider, R., Fiebig, M., and Schluchter, C., (2005) Re-interpretation
940   of the Meikirch pollen record, Swiss Alpine Foreland, and implications for Middle
941   Pleistocene chronostratigraphy. *Journal of Quaternary Science*, 20(6), p. 607-620.
942   Preusser, F., Reitner, J. M., and Schluchter, C., (2010) Distribution, geometry, age and origin
943   of overdeepened valleys and basins in the Alps and their foreland. *Swiss Journal of*
944   *Geosciences*, 103(3), p. 407-426.
945   Preusser, F., and Schlüchter, C., (2004) Dates from an important early Late Pleistocene ice
946   advance in the Aare valley, Switzerland. *Eclogae Geologicae Helvetiae*, 97(2), p.
947   245-253.
948   Pugin, A., Pullan, S. E., and Sharpe, D. R., (1999) Seismic facies and regional architecture of
949   the Oak Ridges Moraine area, southern Ontario. *Canadian Journal of Earth Sciences*,
950   36(3), p. 409-432.
951   Ravazzi, C., Pini, R., Badino, F., De Amicis, M., Londeix, L., and Reimer, P. J., (2014) The
952   latest LGM culmination of the Garda Glacier (Italian Alps) and the onset of glacial
953   termination. Age of glacial collapse and vegetation chronosequence. *Quaternary*
954   *Science Reviews*, 105), p. 26-47.
955   Reber, R., Akçar, N., Ivy-Ochs, S., Tikhomirov, D., Burkhalter, R., Zahno, C., Lüthold, A.,
956   Kubik, P. W., Vockenhuber, C., and Schlüchter, C., (2014) Timing of retreat of the
957   Reuss Glacier (Switzerland) at the end of the Last Glacial Maximum. *Swiss Journal of*
958   *Geosciences*, 107(2), p. 293-307.
959   Reber, R., and Schlunegger, F., (2016) Unravelling the moisture sources of the Alpine
960   glaciers using tunnel valleys as constraints. *Terra Nova*, 28(3), p. 202-211.
961   Reimer, P. J., Bard, E., Bayliss, A., Beck, J. W., Blackwell, P. G., Ramsey, C. B., Buck, C.
962   E., Cheng, H., Edwards, R. L., Friedrich, M., Grootes, P. M., Guilderson, T. P.,
963   Haflidason, H., Hajdas, I., Hatte, C., Heaton, T. J., Hoffmann, D. L., Hogg, A. G.,
964   Hughen, K. A., Kaiser, K. F., Kromer, B., Manning, S. W., Niu, M., Reimer, R. W.,
965   Richards, D. A., Scott, E. M., Southon, J. R., Staff, R. A., Turney, C. S. M., and van
966   der Plicht, J., (2013) Intcal13 and Marine13 Radiocarbon Age Calibration Curves 0-
967   50,000 Years Cal Bp. *Radiocarbon*, 55(4), p. 1869-1887.
968   Reitner, M., Jürgen, Ivy-Ochs, S., Drescher-Schneider, R., Hajdas, I., and Linner, M., (2016)
969   Reconsidering the current stratigraphy of the Alpine Lateglacial: Implications of the
970   sedimentary and morphological record of the Lienz area (Tyrol/Austria). *Quaternary*
971   *Science Journal*, 65(2.
972   Schlüchter, C., (1979) Übertiefte Talabschnitte im Berner Mittelland. *Eiszeitalter und*
973   *Gegenwart*, 29), p. 101-113.
974   Schlüchter, C., (1988) The deglaciation of the Swiss-Alps: A paleoclimatic event with
975   chronological problems. *Bulletin de l'Association francaise pour l'étude du*
976   *Quaternaire*, 25(2), p. 141-145.
977   Schlüchter, C., (1989a) The Most Complete Quaternary Record of the Swiss Alpine Foreland.
978   *Palaeogeography Palaeoclimatology Palaeoecology*, 72(1-2), p. 141-146.
979   Schlüchter, C., (1989b) Thalgut - a Comprehensive Quaternary Record of the Northern Swiss
980   Alpine Foreland. *Eclogae Geologicae Helvetiae*, 82(1), p. 277-284.
981   Schlüchter, C., and Kelly, M., (2000) Das Eiszeitalter in der Schweiz. Eine schematische
982   Zusammenfassung. *Stiftung Landschaft und Kies*, IGCP-378), p. 4.
983   Schnellmann, M., Anselmetti, F. S., Giardini, D., and McKenzie, J. A., (2006) 15,000 Years
984   of mass-movement history in Lake Lucerne: Implications for seismic and tsunami
985   hazards. *Eclogae Geologicae Helvetiae*, 99(3), p. 409-428.

986 van Rensbergen, P., de Batist, M., Beck, C., and Chapron, E., (1999) High-resolution seismic
987 stratigraphy of glacial to interglacial fill of a deep glacigenic lake: Lake Le Bourget,
988 Northwestern Alps, France. *Sedimentary Geology*, 128(1), p. 99-129.
989 Van Rensbergen, P., De Batist, M., Beck, C., and Manalt, F., (1998) High-resolution seismic
990 stratigraphy of late quaternary fill of Lake Annecy (northwestern Alps): evolution
991 from glacial to interglacial sedimentary processes. *Sedimentary Geology*, 117(1), p.
992 71-96.
993 Verschuur, D. J., Berkhout, A. J., and Wapenaar, C. P. A., (1992) Adaptive Surface-Related
994 Multiple Elimination. *Geophysics*, 57(9), p. 1166-1177.
995 Waldmann, N., Ariztegui, D., Anselmetti, F. S., Coronato, A., and Austin, J. A., (2010)
996 Geophysical evidence of multiple glacier advances in Lago Fagnano (54 degrees S),
997 southernmost Patagonia. *Quaternary Science Reviews*, 29(9-10), p. 1188-1200.
998 Welten, M., (1988) Neue pollenanalytische Ergebnisse über das Jüngere Quartär des
999 nordlichen Alpenvorlandes der Schweiz (Mittel-und Jungpleistozän). *Beiträge zur*
1000 *Geologischen Karte der Schweiz*, 162), p. 52.
1001 Widess, M. B., (1973) How Thin Is a Thin Bed. *Geophysics*, 38(6), p. 1176-1180.
1002 Wirsig, C., Zasadni, J., Ivy-Ochs, S., Christl, M., Kober, F., and Schlüchter, C., (2016) A
1003 deglaciation model of the Oberhasli, Switzerland. *Journal of Quaternary Science*,
1004 31(1), p. 46-59.
1005 Wirth, S. B., Girardclos, S., Rellstab, C., and Anselmetti, F. S., (2011) The sedimentary
1006 response to a pioneer geo-engineering project: Tracking the Kander River deviation in
1007 the sediments of Lake Thun (Switzerland). *Sedimentology*, 58(7), p. 1737-1761.
1008 Wissing, S. B., and Pfiffner, O. A., (2002) Structure of the eastern Klippen nappe (BE, FR):
1009 Implications for its Alpine tectonic evolution. *Eclogae Geologicae Helvetiae*, 95(3),
1010 p. 381-398.
1011 Wong, G. S. K., and Zhu, S. M., (1995) Speed of Sound in Seawater as a Function of
1012 Salinity, Temperature, and Pressure. *Journal of the Acoustical Society of America*,
1013 97(3), p. 1732-1736.

1014

1015